Final version published in:
Inorganic Chemistry. 2016, v.55, n.10, p.4850–4863.
https://doi.org/10.1021/acs.inorgchem.6b00359

CF_3 derivatives of the anticancer Ru(III) complexes KP1019, NKP-1339, and their imidazole and pyridine analogues show enhanced lipophilicity, albumin interactions, and cytotoxicity

Stephanie. W. Chang,[†] Andrew R. Lewis,[†] Kathleen E. Prosser,[†] John R. Thompson,[†] Margarita Gladkikh,[†] Marcel B. Bally,[‡] Jeffrey J. Warren,[†] and Charles J. Walsby[†,*]

[†]*Department of Chemistry, Simon Fraser University, 8888 University Drive, Burnaby, BC, Canada, V5A 1S6*

[‡]*Department of Experimental Therapeutics, BC Cancer Agency, Vancouver, BC, Canada, V5Z 4E6*

ABSTRACT: The Ru(III) complexes indazolium [*trans*-$RuCl_4$(1*H*-indazole)$_2$] (KP1019) and sodium [*trans*-$RuCl_4$(1*H*-indazole)$_2$] (NKP-1339) are leading candidates for the next generation of metal-based chemotherapeutics. Trifluoromethyl derivatives of these compounds and their imidazole and pyridine analogues have been synthesized to probe the effect of ligand lipophilicity on the pharmacological properties of these types of complexes. Addition of CF_3 groups also provided a spectroscopic handle for ^{19}F NMR studies of ligand exchange processes and protein interactions. The lipophilicities of the CF_3 functionalized compounds and their unsubstituted parent complexes were quantified by the shake-flask method to give the distribution coefficient at pH 7.4 (log$D_{7.4}$). The solution behavior of the CF_3-functionalized complexes was characterized in phosphate buffered saline (PBS) using ^{19}F NMR, electron paramagnetic resonance (EPR), and UV-Vis spectroscopies. These techniques, along with fluorescence competition experiments, were also used to characterize interactions with human serum albumin (HSA). From these studies it was determined that increased lipophilicity correlates with reduced solubility in PBS but enhancement of non-coordinate interactions with hydrophobic domains of HSA. These protein interactions improve the solubility of the complexes and inhibit the formation of oligomeric species. EPR measurements also demonstrated the formation of HSA-coordinated species with longer incubation. ^{19}F NMR spectra show that the trifluoromethyl complexes release axial ligands in PBS and in the presence of HSA. In vitro testing showed that the most lipophilic complexes had the greatest cytotoxic activity. Addition of CF_3 groups enhances the activity of the indazole complex against A549 non-small cell lung carcinoma cells. Furthermore, in the case of the pyridine complexes, the parent compound was inactive against the HT-29 human colon carcinoma cell line, but showed strong cytotoxicity with CF_3 functionalization. Overall, these studies demonstrate that lipophilicity may be a determining factor in the anticancer activity and pharmacological behavior of these types of Ru(III) complexes.

Introduction

Ruthenium complexes are drawing ever increasing attention as next-generation metal-based anticancer treatments.[1] A particular focus of this development has been classical Ru(III) coordination complexes such as indazolium [*trans*-$RuCl_4$(1*H*-indazole)$_2$] (KP1019, **Figure 1**),[2] sodium [*trans*-$RuCl_4$(1*H*-indazole)$_2$] (NKP-1339, **Figure 1**),[3] and imidazolium [*trans*-$RuCl_4$(1*H*-imidazole)(DMSO-*S*)] (NAMI-A),[4] each of which have demonstrated very promising anticancer activity with low levels of side effects in clinical trials.[3b, 5] Bis-azole complexes such as KP1019 and NKP-1339, and derivatives like imidazolium [*trans*-$RuCl_4$(1*H*-imidazole)$_2$] (KP418, **Figure 1**),[2a, 6] were developed by Keppler and co-workers, with excellent antitumour activity initially identified in murine models.[2a, 7] Currently, NKP-1339 is undergoing clinical development and has shown encouraging results in a phase-I study against a variety of solid tumours.[3b]

While the "Keppler-type" complexes KP1019 and NKP-1339 remain the leading Ru(III) drug candidates against primary tumors, development of new derivatives with different axial heterocyclic ligands is on-going.[8] The ligand exchange rates of Ru(III) complexes are typically sufficiently slow that they can be considered to be kinetically inert.[9] In the case of Keppler-type complexes this means that the axial nitrogen heterocycles usually remain coordinated under physiological conditions and following cellular uptake.[10]

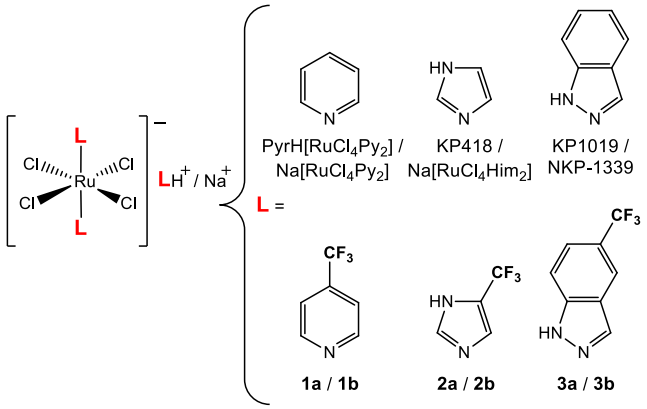

Figure 1. Keppler-type Ru(III) anticancer complexes and new trifluoromethyl derivatives. Compounds **a** compensated by protonated ligands, compounds **b** by sodium counterions.

Consequently, modification of the axial ligands has the potential to influence properties such as aqueous solubility, protein interactions, general cytotoxic activity, and adverse toxicological effects.[3a, 8d, 10b, 10d, 11]

Fluorine substitution is a common strategy in drug development and has been used to improve metabolic stability, enhance binding

to target molecules, and increase lipophilicity and membrane permeability.[12] It has been estimated that 20-25% of drugs under development and as many as 30% of blockbuster pharmaceuticals contain fluorine.[13] Fluorinated compounds have become an important component of the development of new anticancer therapeutics, with the most widely used being 5-fluoropyrimidines such as 5-fluorouracil.[13a, 14] In aromatic systems, such as the ligands of the compounds reported here, replacement of a single hydrogen atom with fluorine typically results in only a modest increase in lipophilicity.[12a] However, addition of a trifluoromethyl group, one of the most lipophilic substituents known, has a much greater effect, and CF_3 has been used as the fluorinated component in a number of pharmaceuticals and drug candidates.[12a, 13a, 13c, 15]

In addition to useful chemical properties, fluorine has also found application in molecular imaging by both ^{19}F magnetic resonance methods[16] and ^{18}F positron emission tomography (PET).[17] NMR studies are facilitated by the favorable properties of the ^{19}F nucleus, which has $I = ½$ and is 100% abundant with a high gyromagnetic ratio, giving high receptivity.[18] ^{19}F also has a broad chemical shift range and this makes it possible to detect subtle changes in the chemical environment of fluorinated compounds.[18] Furthermore, fluorine is essentially absent in biological systems, so NMR spectra can be collected without interference from background signals.[19] Thus, fluorinated reporter molecules can be used in studies of biological processes, using either isolated biomolecules or in vitro/in vivo.[19-20]

Addition of hydrophobic CF_3 groups has the potential to influence the absorption and distribution of the Ru(III) compounds described here by modification of their overall lipophilicity. Previous studies of KP1019 suggest that the complex is taken up by cells both via passive diffusion,[21] and possibly by a pathway mediated by transferrin.[22] Optimal passive transport requires that compounds have sufficiently high lipophilicity to penetrate cell membranes.[12b, 23] However, moderately lipophilic molecules tend to exhibit the best pharmacokinetic properties,[24] since excessively hydrophobic compounds can be trapped within the lipid core of membranes and also exhibit low aqueous solubility. In the case of Keppler-type complexes, the lipophilicity of the axial heterocyclic ligands has been associated with non-coordinate binding to the two principal hydrophobic binding domains of human serum albumin (HSA).[10d, 25] These interactions have been correlated with the low nephrotoxicity of KP1019, as compared to KP418,[11b] since the relatively hydrophobic indazole ligands of KP1019 may enable rapid sequestration of the complex by HSA *in vivo*.[10d] Furthermore, studies of a series of KP1019/NKP-1339 analogues with heterocyclic ligands of varying hydrophobicity showed that this property influenced the stability of non-coordinate interactions with HSA, and affected the activity of protein adducts.[26]

In this study, the synthesis and characterization of trifluoromethyl derivatives of KP1019/NKP-1339, KP418 and their pyridine analogues (**Figure 1**) are reported. We report the influence of the CF_3 groups on the lipophilicity of the complexes, and the impact this has on interactions with HSA and on cytotoxicity activity. Furthermore, we demonstrate the utility of including ^{19}F as an NMR probe of paramagnetic metallopharmaceuticals.

Experimental

Materials: The starting compounds $RuCl_3{\cdot}H_2O$ (Pressure Chemical), 4-(trifluoromethyl)pyridine (Alfa Aesar), 5-(trifluoromethyl)-1*H*-imidazole (Matrix Scientific), and 5-(trifluoromethyl)-1*H*-indazole (Accela BioChem) as well as HSA (Aldrich), 5-fluorouracil (Aldrich), cisplatin (*cis*-diamminedichloridoplatinum(II)) (Sigma-Aldrich), RPMI 1640 media (Gibco), McCoys 5a modified medium (Gibco), L-glutamine (Gibco), fetal bovine serum (Gibco), Hoescht 33342 nucleic acid stain (Life Technologies), and ethidium homodimer I (Biotium) nucleic acid stain were used as purchased. $Na[RuCl_4Py_2]$[8d], $Na[RuCl_4Him_2]$[27] and $Na[RuCl_4Hind_2]$ (NKP-1339)[28] were prepared as described elsewhere.

Crystallographic structure determination: Single-crystal X-ray crystallographic analysis was performed on a Bruker SMART diffractometer equipped with an APEX II CCD area detector fixed at a distance of 5.0 cm from the crystal and a $Mo_{K\alpha}$ fine focus sealed tube (λ = 0.71073 nm) operating at 1.5 kW (50 kV, 30 mA) and filtered with a graphite TRIUMPH monochromator. The structures were solved using the intrinsic phasing method[29] and subsequent refinements were performed using SHELXL[30] within ShelXle.[31] Diagrams of complexes **1a**, **2c**, and **3c** were generated by ORTEP-3[32] and POV-RAY.[33] Crystal data, data collection parameters and details of structure refinement for compounds **1a**, **2c**, and **3c** are listed in **Table S1** in Supporting Information.

NMR measurements: NMR experiments were performed using 5 mm NMR tubes (NewEra HL5) with a co-axial standard capillary (Wilmad, 60 µL) containing 5 mM trifluoroacetic acid (TFA) in D_2O-based phosphate buffered saline (D_2O-PBS). The D_2O-PBS solution contained: NaCl (150 mM), KH_2PO_4 (7.6 mM) and K_2HPO_4 (42.4 mM), pH* 7.4. The pH was measured using a pH probe and was corrected to account for deuterium using the method of Glasoe and Long.[34] Sample tubes were filled with 500 µL of solution to achieve a 50 mm liquid length.

All ^{19}F speciation spectra were measured using a Bruker AVANCE III UltraShield 400WB Plus spectrometer with a BBFO probe, operating at 376 MHz for ^{19}F. Additional ^{19}F NMR spectra of the fluorinated ligands were collected using a Bruker AVANCE III 500 MHz spectrometer with a TXI probe, operating at 470 MHz for ^{19}F. Typical spectral parameters were as follows: spectral width, 60 ppm; acquisition time, 2.88 s; relaxation delay, 0.12 s; number of data points, 128k (zero-filled to 256k), without ^{1}H decoupling. The ^{19}F signal from TFA was used as an external reference for calibrating chemical shifts (peak set to 0 ppm) and D_2O was used as the source of the ^{2}H lock signal. Sample temperatures of 37 °C during NMR experiments were obtained using a flow of heated air over the sample regulated with a Bruker BVT 3000 temperature controller (calibrated using 99.9% CD_3OD).

Complexes in PBS: Complexes **1b** and **2b** were dissolved in D_2O PBS at 37 °C, to give a concentration of 10 mM, and immediately placed in the spectrometer with the probe preheated to 37 °C, and each sample was maintained at this temperature throughout the experiment. During the first 10 minutes of incubation, ^{19}F NMR measurements (20 scans) were made at 2 minute intervals. Subsequently, after 30 min, 1, 2, and 6 h from the time of preparation, measurements were made with 80 scans.

Ligands in PBS: 4-(trifluoromethyl)pyridine, 5-(trifluoromethyl)-1*H*-imidazole, and 5-(trifluoromethyl)-1*H*-indazole were dissolved in D_2O PBS, to give a concentration of 5 mM. Due to lower aqueous solubility, 5-(trifluoromethyl)-1*H*-indazole was dissolved in DMSO then added to D_2O PBS to achieve a concentration of 5 mM in a 25% DMSO solution. ^{19}F NMR measurements (80 scans) were collected at 25 °C.

Complexes with HSA: Complexes **1b**, **2b**, and **3b** (10 mM) and HSA (2 mM) were dissolved together in D_2O PBS at 37 °C. ^{19}F

NMR measurements (80 scans) were performed at 0, 30 min, 1, 2, 6 and 24 h from the time of preparation, with incubation at 37 °C.

Ligands with HSA: The ligands 4-(trifluoromethyl)pyridine, 4-(trifluoromethyl)-1*H*-imidazole, and 5-(trifluoromethyl)-1*H*-indazole (5 mM) and HSA (2 mM) were dissolved in D_2O PBS and incubated at 37 °C for two hours. Due to lower aqueous solubility, 5-(trifluoromethyl)-1*H*-indazole was dissolved in DMSO then added to D_2O PBS to achieve a concentration of 5 mM in a 25% DMSO solution. ^{19}F NMR measurements (80 scans) were collected at 25 °C.

EPR sample preparation: *Complexes in PBS*: Compounds **1b** and **2b** were dissolved in PBS to give a concentration of 3 mM, and incubated at 37 °C for 0, 30 min, 1, 2 and 6 h. The PBS solution contained: NaCl (137 mM), KCl (2.7 mM), Na_2HPO_4 (10 mM), and KH_2PO_4 (2 mM), pH 7.4. After each incubation period, a 210 μL aliquot was taken and mixed with 90 μL of glycerol, which acted as a glassing agent, to produce a final volume of 300 μL, and were then promptly frozen in liquid nitrogen. The low aqueous solubility of **3b** meant it was not possible to obtain an EPR spectrum in PBS.

Complexes with HSA: A solution of HSA (600 μL, 0.75 mM) in PBS was mixed with a 600 μL solution of each complex (1.5 mM), also in PBS. The combined solution was then diluted to 4 mL with PBS and incubated at 37 °C for one of the following time periods: 0, 30 min, 1, 2, 6, and 24 h. Each 4 mL solution was concentrated down to a volume of less than 200 μL using an Amicon centrifugal filter unit (molecular weight cut-off 30 kDa) by centrifuging at 8 °C and 4500 rpm for 30 min, or until a volume of less than 200 μL was attained. The filtered product was then mixed with 90 μL of glycerol and diluted to a final volume of 300 μL with PBS, and frozen in liquid nitrogen.

EPR measurements and simulations: EPR measurements were performed at X-band (9.3–9.4 GHz) using a Bruker EMXplus spectrometer with a PremiumX microwave bridge and HS resonator. Measurements utilized a Bruker ER 4112HV helium temperature-control system and continuous-flow cryostat to maintain a temperature of 20 K. The Bruker cryostat system also enabled reproducible sample placement within the EPR resonator using a quartz-tube holder. Solution conditions and spectroscopic parameters were kept constant for each experiment so that the intensities of the EPR signals from Ru(III)-based species in different samples could be compared. As a result, differences in instrument sensitivity between measurements were minimal, and automatic tuning of the spectrometer gave a Q-factor of 6700 ± 10%. All spectra were simulated using the MATLAB-based program, EasySpin.[35]

Optical measurements: UV-Vis spectra were measured using a Cary1E UV-Visible spectrophotometer, connected to a Haake F3 water bath, which maintained the temperature of each sample at 37 °C. Spectra were collected from the compounds dissolved in PBS. Complexes **2a**,**b** and **3a**,**b** were first dissolved in DMSO to improve solubility then added to PBS, to give a 1% DMSO solution. Measurements were performed on 200 μM solutions of each complex in 1 mL volumes.

Protein binding measurements were performed on 200 μM solutions of each complex with 100 μM HSA in 1 mL volumes. Complexes **2a**,**b** and **3a**,**b** required dissolution in DMSO then addition to PBS to give a 1% DMSO solution to improve solubility. All samples were measured at 37 °C for a total of 2 h with scans taken at 10 min intervals.

Fluorescence competition experiments: Fluorescence competition experiments were performed according to literature procedures.[25] Fluorescence spectra of the sodium-compensated complexes **1b**, **2b**, and **3b** as well as $Na[RuCl_4Py_2]$, $Na[RuCl_4Him_2]$, and $Na[RuCl_4Hind_2]$ (NKP–1339) were recorded at room temperature with a Horiba Fluorolog fluorimeter using entrance and exit slit widths of 5 nm and a 1 cm quartz cell. An excitation wavelength of 335 nm was used in all experiments and emission spectra were collected between 420 and 600 nm. The data were analyzed with Stern-Volmer plots.[36]

A stock solution containing HSA (50 μM) and dansylglycine (50 μM), and a stock solution of each Ru(III) complex (1000 μM) were prepared in a PBS. Complex **3b** and NKP-1339 were dissolved in DMSO to improve solubility then added to PBS to give a 1% DMSO solution. Measurements were performed on 3.5 mL samples containing HSA (1 μM) and dansylglycine (1 μM) with Ru complex concentrations ranging from 0-15 μM.

log$D_{7.4}$ measurements: Distribution coefficients ($D_{7.4}$) were determined by the shake flask method[37] using *n*-octanol and PBS. The sodium-compensated complexes **1b**, **2b**, and **3b,** as well as $Na[RuCl_4Py_2]$, $Na[RuCl_4Him_2]$, and $Na[RuCl_4Hind_2]$ (NKP-1339) were dissolved in *n*-octanol pre-saturated PBS to give 200 μM solutions; **3b** and NKP-1339 were dissolved in DMSO to improve solubility and then added to PBS to give a 1% DMSO solution. The aqueous solutions and *n*-octanol in 1:1 v/v ratio were mixed with an orbital shaker for 2 h at 25 °C. The mixtures were then centrifuged at 5000 rpm for 3 min at 25 °C. UV-Vis spectra were taken at room temperature of the aqueous phase before and after shaking, and the absorbance at λ_{max} was compared to ascertain the value of $D_{7.4}$.

Electrochemical measurements: Cyclic voltammograms were recorded on a CH Instruments 660 potentiostat, equipped with an Ag/AgCl (1 M KCl) reference electrode, a platinum wire counter electrode, and a basal plane graphite working electrode (0.09 cm^2). The basal plane graphite electrode was prepared according to the method of Blakemore et al..[38] $K_3[Fe(CN)_6]$ was used to calibrate the electrode potential. Spectra were collected from 200 μM solutions of the sodium-compensated complexes **1b**, **2b**, **3b**, $Na[RuCl_4Py_2]$, $Na[RuCl_4Him_2]$, and $Na[RuCl_4Hind_2]$ (NKP-1339) in PBS, pH 7.4, with **3b** dissolved in DMSO then added to PBS, giving a 10% DMSO solution, to aid in solubility. Prior to each measurement, samples were deaerated by passing a stream of argon (Praxair, 99.9%) through the solutions for 5 minutes. Measurements were performed at room temperature at a scan rate of 25 mV/s.

Biological activity testing: A549 and HT-29 cells were acquired directly from Dr. Marcel Bally's laboratory (BC Cancer Agency Research Center, Vancouver, BC). A549 cells were cultured at 37 °C under a 5 % CO_2 atmosphere in RPMI 1640 media supplemented with 2 mM L-glutamine and 10% fetal bovine serum. HT-29 cells were cultured at 37 °C under a 5 % CO_2 atmosphere in McCoy's 5a modified medium supplemented with 1.5 mM L-glutamine and 10% fetal bovine serum. The sodium-compensated complexes **1b**, **2b**, and **3b**, $Na[RuCl_4Py_2]$, $Na[RuCl_4Him_2]$, and $Na[RuCl_4Hind_2]$ (NKP-1339), as well as cisplatin were diluted from 10 mM stocks in DMSO to give the desired concentrations in complete cellular media for cytotoxicity testing. To verify that the compounds would remain soluble under assay conditions, each compound was incubated in complete cell media at the maximum testing concentrations for 72 hours at 37 °C and in each case there was no evidence of precipitation.

For in vitro cytotoxicity assays, A549 and HT-29 cells were seeded in quadruplet at 2000 cells/well and 3000 cells/well, respective-

ly, in 384-well plates (Grener Bio-One). Following a 24 h incubation period, 20 µL aliquots of each complex in media were added to each well to give the desired concentration with a DMSO concentration of 1%. Wells containing a media control and a vehicle (DMSO) control were also prepared. After 72 h of treatment with each complex, the cells were stained using 5 µL of a 10 mg/mL stock of Hoescht 33342 nucleic acid stain and 3 µL of a 1 mM stock of ethidium homodimer I per mL of media. These stains generate a total cell count and a dead cell count respectively. After a 20 minute incubation period the plates were then imaged using an IN Cell Analyzer 1000 (GE Healthcare), which is an automated fluorescent microscopy platform that enables high-content screening. Cell counts were determined via the IN Cell Developer Toolbox software. Cells were classified as "dead" if they showed > 30% overlap of the two stains. Statistical analyses to determine half maximal inhibitory concentrations (IC_{50}) were performed using GraphPad software.

Synthesis:

(4-(CF_3)Py)$_2$H[trans-RuCl$_4$(4-(CF_3)Py)$_2$] (**1a**). $RuCl_3 \bullet H_2O$ (0.207 g, 1 mmol) was dissolved in ethanol (6 mL) and HCl (1 M, 6 mL) and refluxed for 3 hours to produce a clear, brown-orange solution. Half of the solvent was then removed by rotary evaporation. 4-(trifluoromethyl)pyridine (0.6950 mL, 6 mmol) was dissolved in ethanol (1.5 mL) and HCl (6 M, 1.5 mL), and added to the Ru solution. This combined solution was then refluxed for 30 minutes to give **1a** as a fine orange powder. The product was isolated by gravity filtration and washed with cold ethanol (3 × 2 mL). X-ray quality crystals were recovered from the filtrate after it was stored at −18 °C for several days. Yield: 47.8%, Mel. Temp. 230 °C (decomp.), $C_{24}H_{17}Cl_4F_{12}N_4Ru$ Calc. C, 34.64; H, 2.06; N, 6.73. Found C, 34.49; H, 2.05; N, 6.67. ^{1}H NMR (DMSO): δ = 8.81, 7.73, −5.07. ^{19}F NMR (MeOD): δ = −63.53, −77.64.

Na[trans-RuCl$_4$(4-(CF_3)Py)$_2$]•H_2O (**1b**). **1a** (0.0343 g, 0.041 mmol) was suspended in dried DCM (6 mL). $NaBPh_4$ (0.171 g, 0.5 mmol) was dissolved in dry acetone (1 mL) and added dropwise to the **1a** suspension to produce an orange solution. The solution was stirred at room temperature for 1.5 h and then diethyl ether (4.5 mL) was added and the solution was then allowed to stir for 17 h. The desired product **1b** was formed as a fine yellow-orange powder, which was isolated by filtration and washed with diethyl ether (3 × 2 mL). Under ambient conditions the dry precipitate turned green after about 24 hours, but this process was slowed in a desiccator; this color change did not cause any alteration to either the intensity or appearance of the EPR or NMR spectra of the compound. Yield: 58.5%, Mel. Temp. 138 °C (decomp.), $C_{12}H_9Cl_4F_6N_2NaORu$ Calc. C, 24.93; H, 1.74; N, 4.85. Found C, 24.80; H, 1.89; N, 4.85. ^{1}H NMR (D_2O): δ = −6.08, ^{19}F NMR (D_2O): δ = −75.77.

4-(CF_3)H_2Im[trans-RuCl$_4$(5-(CF_3)Him)$_2$]•H_2O (**2a**). $RuCl_3 \bullet H_2O$ (0.208 g, 1 mmol) was dissolved in ethanol (5 mL) and HCl (1 M, 5 mL). The solution was refluxed for 3 hours, resulting in a clear, brown-orange solution, which was then concentrated to minimum solvent volume and additional HCl (1 M, 0.7 mL) was added. This Ru solution was then added to 4-(trifluoromethyl)-1*H*-imidazole (0.5444 g, 4 mmol) dissolved in HCl (6 M, 0.3556 mL). The resulting solution was stirred at 60 °C for 10 min resulting in the formation of the product **2a** as an orange-red powder, which was recovered by gravity filtration and washed with DCM (3 × 2 mL). Yield: 44.5%, Mel. Temp. 189 °C (decomp.), $C_{12}H_{12}Cl_4F_9N_6ORu$ Calc. C, 21.51; H, 1.81; N, 12.54. Found C, 21.52; H, 1.65; N, 12.71, ^{1}H NMR (MeOD): δ = 8.68, 8.06, −16.35, −17.62, ^{19}F NMR (MeOD): δ = −63.01, −68.40.

Na[trans-RuCl$_4$(5-(CF_3)Him)$_2$]•2.5H_2O (**2b**). **2a** (0.0494 g, 0.075 mmol) was dissolved in cold acetone (1.5 mL) and $NaBPh_4$ (0.0299 g, 0.875 mmol) was also dissolved in cold acetone (1.5 mL). The $NaBPh_4$ solution was added dropwise to the solution of **2a** to give an orange solution, which was stirred for 2 hours to give a color change to brown. An excess of diethyl ether (50 mL) was added to give the product **2b** as a dark red-brown precipitate that was recovered via gravity filtration and washed with diethyl ether (2 × 2 mL). Yield: 34.4%, Mel. Temp. 140 °C (decomp.), $C_8H_{11}Cl_4F_6N_4NaO_{2.5}Ru$ Calc. C, 16.48; H, 1.90; N, 9.61. Found, C, 16.87; H, 2.35; N, 9.51. ^{1}H NMR (MeOD): δ = −16.30, −17.64, ^{19}F NMR (MeOD): δ = −68.41.

PPh$_4$[trans-RuCl$_4$(5-(CF_3)Him)$_2$] (**2c**). **2a** (0.1400 g, 0.2144 mmol) was dissolved in methanol (4.5 mL) and tetraphenylphosphonium chloride (PPh_4Cl) (0.760 g, 2.075 mmol) was then added directly to the solution. The resulting orange solution was stirred for 45 minutes at room temperature and then cooled to −18 °C for 1 h. Diethyl ether was added until **2c** was produced as a fine orange precipitate, which was then recovered by filtration and washed with diethyl ether. X-ray quality crystals were recovered from the reaction filtrate after several days at −18 °C. Yield: 49.7%, Mel. Temp. 235 °C (decomp.), $C_{32}H_{26}C_{l4}F_6N_4RuP$ Calc. C, 44.98; H, 3.07; N, 6.56. Found C, 45.11; H, 2.96; N, 6.68., ^{1}H NMR (MeOD): δ = 7.97, 7.80, −16.31, −17.70, ^{19}F NMR (MeOD): δ = −68.41.

5-(CF_3)H_2In[trans-RuCl$_4$(5-(CF_3)Hin)$_2$]•4H_2O (**3a**). $RuCl_3 \bullet H_2O$ (0.057 g, 0.272 mmol) was dissolved in ethanol (1.5 mL) and HCl (12 M, 1.5 mL) and was refluxed for 3 hours resulting in a clear, brown-orange solution. This solution was then concentrated by removal of two thirds of the solvent via rotary evaporation. 5-(trifluoromethyl)-1*H*-indazole (0.2023 g, 1.087 mmol) was dissolved in HCl (12 M, 3 mL, 60-70 °C) and then combined with the Ru solution and subsequently stirred at room temperature for 15 min. The product was produced as an orange-brown precipitate and was collected by gravity filtration, washed with water (3 × 2 mL) and then allowed to air dry overnight. The product was then washed with diethyl ether (50 mL) to give **3a** as a pure light sandy orange solid. Yield: 50%, Mel. Temp. 162 °C (decomp.), $C_{24}H_{24}Cl_4F_9N_6O_4Ru$ Calc. 32.97; H, 2.77; N, 9.61. Found, C, 33.04; H, 2.88; N, 9.66. , ^{1}H NMR (MeOD): δ = 8.22, 8.18, 8.12, 7.71, 7.70, 7.63, 7.62, 1.59, −0.03 ^{19}F NMR (MeOD): δ = −62.44, −64.99.

Na[trans-RuCl$_4$(5-(CF_3)Hin)$_2$]•2H_2O•(CH_3CH_2)$_2O$ (**3b**). **3a** (0.0166 g, 0.0207 mmol) was suspended in dichloromethane (5 mL). $NaBPh_4$ (0.0303, 0.0886 mmol) was dissolved in acetone (3 mL) and added dropwise to the solution of **3a**. The resulting solution was refluxed for 1.5 hours to give a color change to dark red. After concentrating to a minimum solvent volume by rotary evaporation, the resulting red-brown oil was dissolved in acetonitrile (0.5 mL) and then dichloromethane (3 mL) was added. Hexanes (6 mL) was added to this solution after which it became cloudy. After the solution was kept at −18 °C for 16 hours, a red-brown precipitate was collected by gravity filtration. The precipitate was dissolved in diethyl ether (4 mL) for recrystallization. The solution was separated from an insoluble side-product and then allowed to evaporate under ambient conditions. **3b** was collected as a red-brown crystalline solid. Yield: 11.2%, Mel. Temp. 122 °C (decomp.), $C_{16}H_{29}Cl_4F_6N_4NaO_3Ru$ Calc. C, 32.10; H, 3.23; N, 7.49.

Found C, 31.91; H, 3.32; N, 7.11. ^{1}H NMR (MeOD): δ = 8.09, 1.59, –0.03, ^{19}F NMR (MeOD): δ = –64.44.

PNP[trans-RuCl$_4$(S-(CF$_3$)Hin)$_2$] (**3c**). **3a** (0.0333 g, 0.0141 mmol) was dissolved in acetone (4 mL). Bis(triphenylphosphine)iminium (PNP) chloride (0.0238 g, 0.0414 mmol) was added directly to the solution of **3a**, and the combined solutions were stirred for 1 h at 60 °C, after which diethyl ether (50 mL) was added to produce an orange suspension. A fine sandy orange precipitate was collected by gravity filtration and washed with diethyl ether (2 × 2 mL). X-ray quality crystals were recovered from the filtrate after 2 weeks at room temperature. Yield: 12.5%, Mel. Temp. 117-122 °C, $C_{52}H_{40}Cl_4F_6N_5P_2Ru$ Calc. C, 54.13; H, 3.49; N, 6.07. Found C, 54.05; H, 3.67; N, 5.96. ^{1}H NMR (MeOD): δ = 7.68, 7.60, 7.52, 4.59, 2.68, 1.48, ^{19}F NMR (MeOD): δ = –65.28.

Results and discussion

Synthesis: Compounds **1a**,**b**, **2a**,**b**,**c**, and **3a**,**b**,**c** were synthesized using procedures derived from the original syntheses of KP1019, NKP-1339, KP418, and their respective sodium and tetraphenylphosphonium (PPh_4^+) compensated derivatives.[6, 8d, 28, 39] The identity and purity of the compounds were confirmed by elemental analysis, NMR (^{1}H and ^{19}F), and EPR spectroscopies, as well as X-ray crystallographic analyses.

Crystal structures: The sodium compensated complexes **1b**, **2b**, and **3b** were used for speciation and biological studies due to their solubility in PBS. However, X-ray quality crystals of these compounds could not be obtained. Crystals were obtained for the CF$_3$-Py complex with a CF$_3$-pyridinium-CF$_3$-pyridine cation (**1a**), the CF$_3$-Him complex with PPh_4^+ (**2c**), and the CF$_3$-Hin complex with PNP^+ (**3c**). The structure of the cation of **1a** is consistent with that determined crystallographically for the pyridinium-pyridine cation, which has been characterized as a pair of pyridine molecules linked by hydrogen bonding between their nitrogen atoms and a shared proton.[40] The structures of the anions of these compounds as determined by X-ray crystallography are shown in **Figure 2**.

Comparison of the structures of each complex with the unsubstituted parent compounds shows that addition of the CF$_3$ groups does not significantly affect the ligand coordination to the Ru centers. In all cases, the heterocyclic ligands are coordinated through their nitrogen atoms in a trans arrangement with four equatorial chlorine ligands completing the coordination sphere. The Ru–N and Ru–Cl bond lengths of **1a**, **2c**, and **3c** (**Table S2**) are very similar to those reported for their respective parent compounds.[8d, 27-28]

Lipophilicity (log*D*$_{7.4}$) measurements: The axial heterocyclic ligands of Keppler-type complexes influence their solution behavior and interactions with biomolecules.[8d, 10d] In particular, the ligands can modulate the overall lipophilicity of the complexes. Lipophilicity is an important general determinant of the pharmacokinetic behavior of successful drugs,[41] and is commonly quantified in terms of the water-octanol partition coefficient (log*P*).[42] When charged species are involved, such as the anions of KP1019, NKP-1339, and their derivatives, lipophilicity can be defined at a specific pH by a distribution coefficient (log*D*).[42-43] Various structure-pharmacokinetic studies have provided quantitative correlations between lipophilicity and "druglikeness," such as Lipinski's observation that a value of log*P* less than 5 is optimal for oral bioavailability.[44] Although current treatment protocols used in clinical trials of KP1019 and NKP-1339 employ intravenous administration,[3b] lipophilicity remains a key factor in the bioavailability of these types of complexes, defining solubility and interactions with biomolecules in vivo.[8d, 10d]

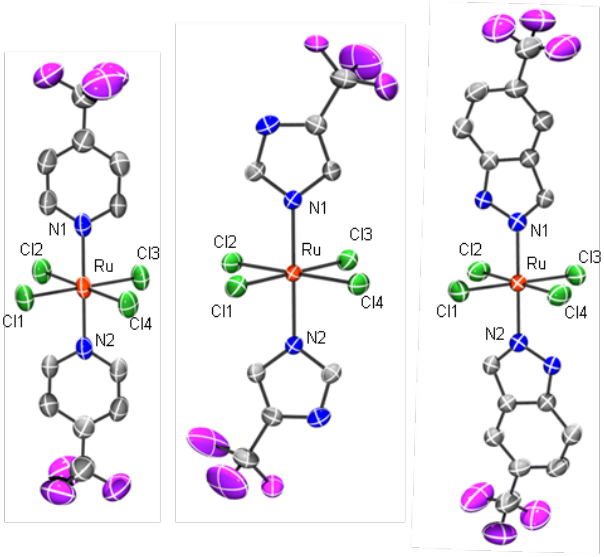

Figure 2. Crystal structures of the anions of complexes **1a**, **2c**, and **3c**. For clarity, the counterions and co-crystallizing solvent molecules for each complex are omitted. Structures are drawn at the 50% probability level.

Complexes **1b**, **2b**, **3b**, and their parent compounds, Na[RuCl$_4$Py$_2$], Na[RuCl$_4$Him$_2$], and Na[RuCl$_4$Hin$_2$] (NKP-1339), were dissolved in PBS at room temperature. Complexes **3b** and NKP-1339 required 1% DMSO to improve initial aqueous solubility. The value of the distribution coefficient at pH 7.4 (log$D_{7.4}$) was determined by measuring the UV-Vis spectrum of the aqueous phase before and after shaking with *n*-octanol. The difference in absorbance at λ_{max} correlates with the change in concentration in the aqueous phase due to partitioning into the *n*-octanol layer, with $D_{7.4}$ calculated according to Equation 1:[37b]

$$D_{7.4} = \frac{[n\text{-octanol}]}{[\text{PBS}]} = \frac{\text{Abs at } \lambda_{max} \text{ (before shaking)}}{\text{Abs at } \lambda_{max} \text{ (after shaking)}} - 1 \qquad (1)$$

The typical shake-flask protocol uses 24 hours of mixing prior to the measurement of concentration in each layer. However, to minimize the effects of ligand-exchange processes, a shorter mixing time of 2 hours was used in these experiments. Aquation of all of the complexes occurs readily at 37 °C, but UV-Vis spectra collected at room temperature show that a negligible amount of ligand exchange occurs during two hours in PBS (**Figures S28**-**S33**). Thus, all log$D_{7.4}$ measurements were performed at this temperature. The lipophilicity of the fluorinated chemotherapeutic 5-fluorouracil was also measured by this procedure, giving a log$D_{7.4}$ value of –0.88. This is in close agreement with the reported log*P* value of –0.79,[45] demonstrating that our protocol gives values that are relevant for comparison to other literature studies of drug lipophilicity.

Table 1: Distribution coefficients (log$D_{7.4}$), conditional HSA binding constants at site II (logK'), formal potentials ($E°'$), and IC_{50} values for Keppler-type complexes and CF_3 functionalized derivatives. log$D_{7.4}$, logK', and formal potential measurements were collected at room temperature.

Complex	log$D_{7.4}$	logK'	$E°'$ (mV)	IC_{50} (μM)	
				HT-29	A549
$Na[RuCl_4(CF_3Hin)_2]$ (**3b**)	~1.4 [a]	5.79 [a]	218 [b]	24(4)	21(4)
$Na[RuCl_4(CF_3Py)_2]$ (**1b**)	0.38	5.16	232	21(3)	>100
NKP-1339	0.27 [a]	5.05 [a]	17	10(1)	50(23)
$Na[RuCl_4(CF_3Him)_2]$ (**2b**)	−0.59	4.65	−141	>100	>100
$Na[RuCl_4Py_2]$	−1.12	3.94	−43	>100	>100
$Na[RuCl_4Him_2]$	−1.28	4.07	−188	>100	>100
Cisplatin	--- [c]	--- [c]	--- [c]	9(4)	5(1)

[a]Compound **3b** and NKP-1339 were measured in a 1% DMSO PBS solution.

[b]Corrected $E°'$ value since compound **3b** was measured in a 10% DMSO PBS solution, see main text for correction method.

[c]Parameter not measured for cisplatin.

The values of log$D_{7.4}$ for both the parent Keppler-type complexes and their CF_3 functionalized derivatives are shown in **Table 1**. In both series of compounds the lipophilicity increases according to the type of heterocyclic ligands with indazole > pyridine > imidazole. Furthermore, the CF_3 groups of **1b**, **2b**, and **3b** increase their lipophilicity relative to their unsubstituted parent compounds. Thus, overall **3b** is the most lipophilic of all the compounds and only a small remnant of the signal from this compound could be detected in PBS after mixing (**Figure S3**) giving an approximate value of log$D_{7.4}$ ~1.4. Of the other complexes, **1b** (log$D_{7.4}$ = 0.38) and NKP-1339 (log$D_{7.4}$ = 0.27) show the highest lipophilicity.

As we show below, the lipophilicity of the compounds correlates with their solubility, interactions with HSA, and cytotoxicity. This demonstrates quantitatively the importance of this property to key aspects of the behavior of these types of complexes.

Aqueous solution behavior: The solution behavior of KP1019 and NKP-1339 has been thoroughly investigated using a variety of techniques.[2b, 5b, c, 10c, d, 11c, 21b] Under physiological aqueous conditions, KP1019 forms an insoluble monoaqua species that precipitates out of solution within minutes.[10c, 46] While this has not prevented KP1019 from performing well in clinical trials,[2b, 3a, 5b, c, 11a, 47] the alternative formulation with a sodium counterion, NKP-1339, has greater solubility, and is currently under active clinical development.[3b, 48] The bis- imidazole complex, KP418 is more soluble and undergoes step-wise ligand exchange to produce several aquated species under physiological conditions.[9a, 27] This demonstrates the role that the axial ligands play in the solution behavior of these types of compounds. As shown below, modification of these ligands with CF_3 groups has a distinct effect on how the complexes behave in PBS.

^{19}F NMR. Each of the CF_3 modified complexes has six equivalent ^{19}F nuclei. This is advantageous for NMR studies since, combined with the high receptivity of ^{19}F, this gives high signal-to-noise. Furthermore, a single ^{19}F NMR signal is observed from each species in solution, which simplifies speciation studies. These properties are particularly important for the complexes in this study since they contain a paramagnetic Ru(III) (d^5, low spin, S = ½) center that causes line broadening.

Complexes **1b** and **2b** were dissolved in PBS (10 mM), and ^{19}F NMR spectra were collected at selected time points during 6 hours of incubation at 37 °C. Incubation of complex **3b** at 37 °C resulted in rapid precipitation, so NMR studies of its behavior in PBS could not be conducted. A blue-green precipitate formed within 10 minutes, which is likely due to formation of insoluble polynuclear species, analogous to that observed for KP1019 under similar conditions.[10c]

Initially, **1b** shows a strong signal at 0.38 ppm (**Figure 3**). After 10 mins of incubation a second species (δ = 1.72 ppm) is predominant, and further incubation generates three more signals (δ = 3.26, 0.93 and −0.02 ppm). These signals are consistent with mononuclear paramagnetic Ru(III) species, demonstrating stepwise aquation in PBS. Similar behavior has been reported from other Keppler type complexes, such as KP418.[10d, 49] From 30 minutes onwards, there was a steady decrease in overall signal intensity due to precipitation. This coincided with the appearance of new peaks in the range of 6.9 to 10.8 ppm (**Figure S12**), which are likely due to soluble aggregate and oligomeric species. After 1 h of incubation a distinct peak at 10.60 ppm was also observed, which correlates with the chemical shift of free CF_3-Py, as determined separately under the same solvent conditions (PBS, pH 7.4*, 37 °C, **Figure S15a**, δ = 10.58 ppm). This suggests that loss of the ligand under physiological conditions follows the formation of aggregates and oligomeric species.

When dissolved in PBS, complex **2b** initially exhibits a single peak at 13.49 ppm (**Figure S13**). With incubation at 37 °C this signal shifts upfield. However, no other paramagnetic Ru(III) species were observed until 6 hours of incubation, when a secondary broad peak at δ = 11.74 ppm became evident. A sharp signal at

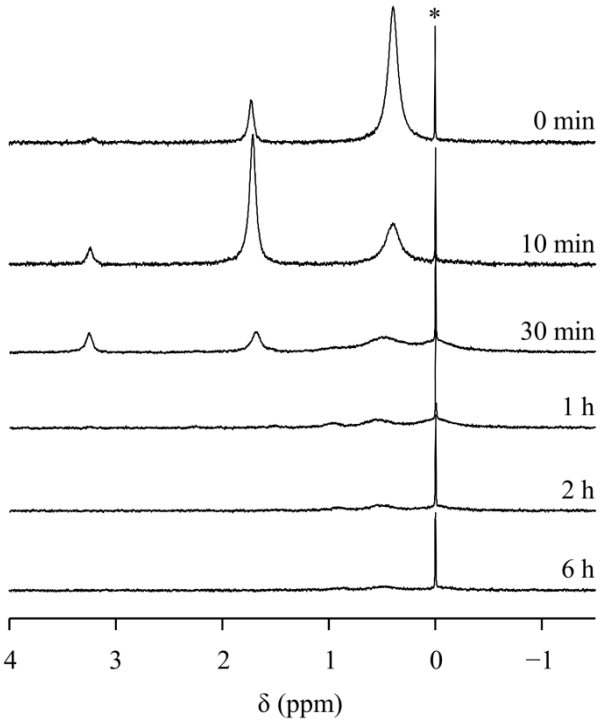

Figure 3. ^{19}F NMR spectra of **1b** (10 mM) incubated in PBS at 37 °C for 6 hours. Chemical shifts calibrated using an external trifluoroacetic acid signal indicated by "*".

13.74 ppm was also observed, which grew in intensity with incubation. This second signal arises from free CF_3-Him, as determined by an independent measurement of the ligand under the same solvent conditions (PBS, pH 7.4*, 37 °C, **Figure S15b,** δ = 13.66 ppm). Thus, the second Ru(III) species observed is likely a species generated by loss of a CF_3-Him ligand. These observations demonstrate distinct differences in solution behavior as compared to **1b**, reflecting the influence of their axial ligands on these processes.

Exchange of a CF_3Py from **1b**, and CF_3-Him from **2b**, although not dominant processes in solution, still has the potential to impact on their pharmacological properties. The bis-imidazole complex, KP418, is known to exchange an imidazole ligand under biologically relevant conditions (pH 7.4, 37 °C),[39] but not in aqueous solution alone.[9a] As determined from analysis of the electrochemical properties of these compounds (see below), the addition of CF_3 groups makes the ligands less electron donating, likely leading to weaker Ru-N bonds and promoting ligand exchange.

EPR. The complexes in this study have paramagnetic Ru(III) (d^5, low spin, S = ½) centers, so changes to their coordination environment can be studied readily using EPR. This approach has been used in previous studies of Keppler-type complexes, to characterize their ligand-exchange processes.[8d, 10d, 21b] In this work, complexes **1b** and **2b** were dissolved in PBS and incubated for up to 6 hours. At selected time points, aliquots were extracted, frozen, and EPR measurements were made. The solution stability of **3b** was not sufficient to obtain EPR data, due to rapid precipitation under these conditions. The spectra of **1b** (**Figure 4**) and **2b** (**Figures 8**, **S5**) at different time points exhibit signals from multiple components, as well as intensity changes with incubation. These data were analyzed by spectral deconvolution using weighted combinations of individual simulated spectra, as shown in **Figure 4** and Supporting information **Figures S6** and **S7**.

For **1b**, the multiple ligand-exchange processes detected by ^{19}F NMR are also evident in the EPR spectra of the complex (**Figure 4**). Prior to incubation, a spectrum comprised of two components, a uniaxial signal with $g_\perp$ = 2.71 and $g_{||}$ = 2.35, and a rhombic signal with g = [2.65, 2.52, 2.29] (**Figure S6a**) was observed. This is consistent with previous EPR studies of KP1019 and KP418, which also show two-component spectra immediately after dissolution in aqueous solution.[10d] With incubation at 37 °C, the original signals from **1b** were steadily replaced by signals from ligand exchange products. The first of these (1b-C3), with g = [2.58, 2.28, 1.71], was visible during the first 30 minutes of incubation, after which its signal was subsequently attenuated. At longer incubation times the spectra are dominated by signals from two species with g = [2.35, 2.33, 2.09] (1b-C4) and g = [2.28, 2.24, 1.95] (1b-C5). In addition, an overall reduction in intensity was observed, consistent with formation of polynuclear species. Coupling between adjacent Ru(III) centers in these species, either antiferromagnetic (S = 0, EPR silent) or ferromagnetic (S > ½) means they are not detected in these experiments.

The EPR spectra from **2b** (**Figures 8a, S5**) are also composed of a uniaxial component, $g_\perp$ = 2.64 and $g_{||}$ = 2.14, and a rhombic component simulated with g = [2.94, 2.30, 1.10] (**Figure S7**). The low-field g value was not observed for the second species, so a value similar to that reported for KP1019 and KP418[10d] with a large line width was used in spectral simulations. With these parameters, the g_3 peak did not impact the simulation in the experimentally measured region. The overall shape of the EPR spectrum of **2b** is essentially unchanged even after extended incubation at 37 °C. This indicates that the species initially detected remain the dominant Ru(III) compounds in solution, which is consistent with the ^{19}F NMR data. The species generated by loss of an axial CF_3Him ligand identified by NMR, is tentatively assigned to a broad feature at 1800 G visible in the EPR spectra at incubation times of 1 h onwards. A weak signal from this species is also in accord with the NMR data. As with **1b**, the overall reduction in EPR signal intensi-

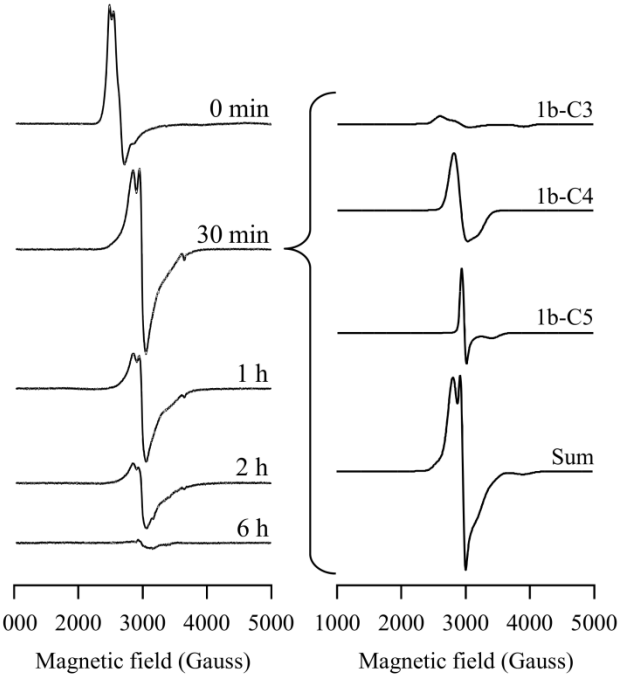

Figure 4. EPR spectra of **1b** (3mM) in PBS with incubation at 37 °C, and deconvolution of 30 min spectrum by simulation.

ty observed with incubation is likely due to precipitation and formation of EPR-silent, soluble polynuclear species. For **2b**, precipitation is accompanied by a solution color change from orange-brown to dark blue.

UV-Vis. The complexes **1a**,**b**, **2a**,**b**, and **3a**,**b** were dissolved in PBS, and UV-Vis spectra were collected at 10 minute intervals over two hours of incubation at 37 °C. In each case the different counterions, sodium or protonated ligand, did not strongly influence the appearance of the spectra.

Consistent with the NMR and EPR experiments, **1a**,**b** show UV-Vis spectral changes reflecting ligand-exchange processes. Initially a peak at λ = 368 nm, likely arising from a ligand-to-metal charge transfer (LMCT) transition, and absorbances at 261 and 325 nm, which are assigned to ligand-based transitions, were observed (**Figure 5**, **Figure S16**). Similar spectra and transition assignments have been reported for $Na[RuCl_4Py_2]$.[8d] With incubation, the LMCT band decreases in intensity and a new absorbance at λ = 345 nm grows in intensity, reflecting ligand exchange processes. The spectra of **2a**,**b** and **3a**,**b** (**Figures S18-S21**) show baseline increases and the appearance of a broad band at 550 nm, which indicate aggregation of the complexes. Overall, the UV-Vis measurements show that the heterocyclic CF_3 ligands influence the solution behavior of the complexes, particularly their solubility.

Interactions of Complexes with HSA: Albumin is the most abundant protein in the circulatory system and has been identified as the primary transporter of many drugs, particularly following intravenous administration.[50] A number of studies have demonstrated that HSA has a high affinity for Ru(III) complexes, [51] and it has been identified as the main transport protein for KP1019 and NKP-1339 in vivo.[3b] HSA has two principal hydrophobic binding regions, site I and site II, which are located in subdomains IIA and IIIA of the protein respectively,[52] and are potential sites for non-coordinate interactions with Keppler-type complexes.[25] Furthermore, coordination to amino acid side chains may occur, most likely with histidine imidazoles.[10a, 53] Both coordinate and non-coordinate interactions of Keppler-type compounds with HSA have been reported and are prevalent under physiological conditions.[3b, 8d, 10d] In the case of KP1019 it has been shown that the complex forms non-coordinate interactions with the HSA initially, but

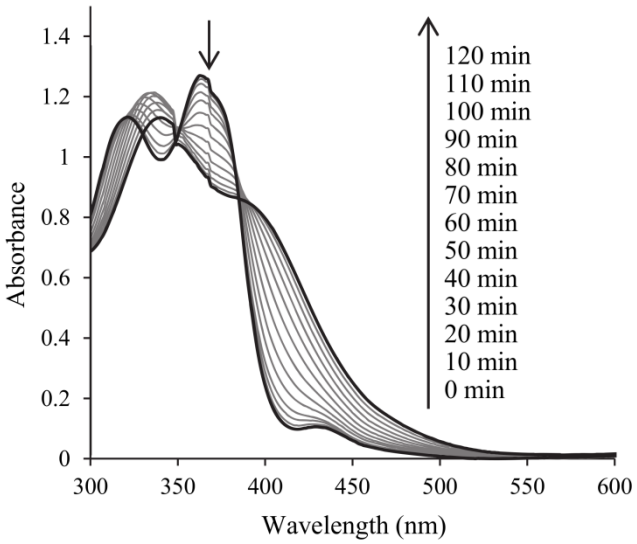

Figure 5. UV/Vis spectrum of complex **1b** (200 μM) in PBS pH 7.4 solution at 37 °C over two hours.

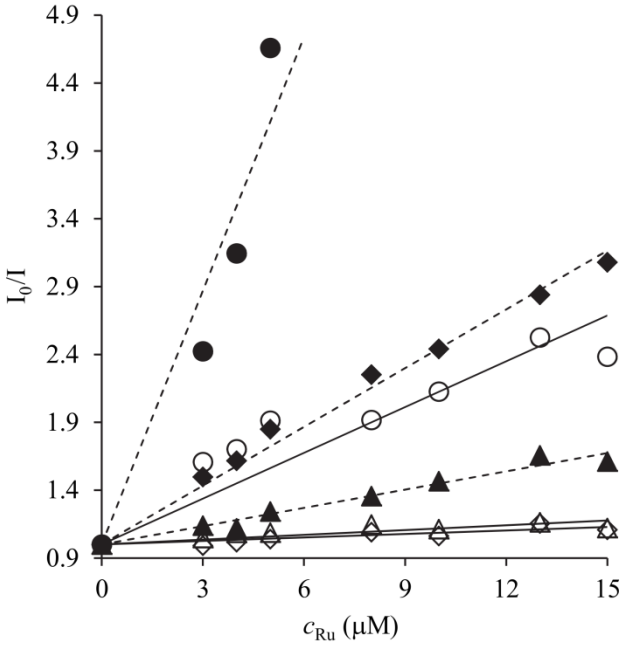

Figure 6. Stern-Volmer plot of fluorescence competition experiments for complexes **1b** (◆), **2b** (▲), and **3b** (●) and their unfluorinated counterparts $Na[RuCl_4Py_2]$ (◇), $Na[RuCl_4Him_2]$ (△), and NKP-1339 (○). Fluorinated complex trend lines are dashed while unfluorinated complex trend lines are solid. Experimental conditions: c_{HSA} = c_{DG} = 1 μM, c_{Ru} = 0-15 μM; excitation wavelength = 335 nm; emission wavelength = 478 nm; ambient temperature; pH 7.4.

coordinates to the protein after longer time periods.[10d]

Fluorescence competition experiments. Fluorescence competition experiments were used to assess the effect of the CF_3 groups of **1b**, **2b**, and **3b** on interactions with HSA. This approach allows quantification of the interactions of molecules with either of the two primary hydrophobic binding sites of the protein.[52] Displacement of a fluorophore with a specific affinity for one of these sites by a competing compound can be assessed by titration to yield a conditional binding constant, *K′*, which is a measurement of the compound's binding strength to that particular hydrophobic domain. This approach has been used previously for KP1019 and NKP-1339, demonstrating interactions with both sites I and II.[25] However, this earlier study showed that KP1019 and NKP-1339 have no preference for site I or II,[25] and in the experiments performed here only interactions with site II have been studied.

An established marker for site II is the fluorophore dansylglycine (DG),[52] which fluoresces strongly in the region of 390-600 nm when in the hydrophobic environment of site II. When displaced into hydrophilic media, such as PBS, the fluorescence intensity of DG is diminished and red shifted to 540 nm. Therefore, a decrease in the fluorescence intensity from the HSA-DG adduct can be correlated with the displacement of DG from site II by a competitor such as a Ru(III) complex. *K′* can be determined using the Stern-Volmer relationship (Equation 2), where I_0 is the initial intensity of fluorescence when the competitor concentration c_{Ru} = 0 μM, and I is the intensity of fluorescence for c_{Ru} > 0 μM.[25]

$$\frac{I_0}{I} = 1 + K'c_{Ru} \qquad (2)$$

I_0/I was determined at various HSA to competitor ratios and then plotted against c_{Ru}. This is a linear relationship in the presence of a single fluorophore, as is the case here for each of the Ru(III) com-

plexes studied.[36] From Equation 2, the conditional binding constant at site II, K', was determined from the slope of the line of the resulting plot of I_0/I vs. c_{Ru} (**Figure 6**).

Fluorescence competition experiments were performed for **1b**, **2b**, and **3b** and their parent compounds Na[$RuCl_4Py_2$], Na[$RuCl_4Him_2$] and NKP-1339. The values of logK' for each compound are shown in **Table 1**, and our logK' value for NKP-1339 (5.03) compares well with the literature value (5.32).[25] Comparison of the binding constants of each of the compounds shows that the addition of the CF_3–modified ligands increases the affinity of the complexes for site II of HSA. Furthermore, there is a good correlation between the values of log$D_{7.4}$ and logK', demonstrating that the affinity of the site for compounds is modulated by hydrophobicity. The ordering of the affinities for HSA site II, **3b** > **1b** > NKP-1339 > **2b** > Na[$RuCl_4Py_2$] > Na[$RuCl_4Him_2$], reflects the combined contributions of the heterocyclic axial ligands and the CF_3 groups on the overall hydrophobicity of the complexes. Notably, **3b** presents a significantly higher logK'than any of the other compounds, which we attribute to its very hydrophobic CF_3-Hin ligands. This also meant that at concentrations higher than 5 μM, the concentration of displaced DG was sufficiently high that it contributed significantly to the fluorescence intensity measurement, and so data above this concentration were not used in the calculation of logK'. We note that for each complex the species displacing DG may include any of those generated by ligand exchange processes. However, UV-Vis measurements (see below), demonstrate greater solubility of all of the complexes in the presence of HSA, indicating that aggregated polynuclear species are less likely to be involved.

^{19}F NMR. Complexes **1b**, **2b**, and **3b** were incubated with HSA at 37 °C for 24 hours (**Figures 7, S14**). These solutions were prepared with a fivefold excess of the ruthenium complexes to achieve higher concentrations of protein bound species and therefore allow ^{19}F NMR spectra with a suitable signal-to-noise ratio to be obtained. However, sample spectra collected with a twofold excess, as used in the EPR and UV-Vis experiments, showed the same spectral features.

The ^{19}F NMR spectra of **1b** with HSA (**Figure 7**) show distinct differences from those of the complex in PBS. Although the general spectral appearance below 5 ppm is reminiscent of the PBS studies, the peaks are shifted upfield and broadened in the presence of the protein. Initially, a broad peak is observed at −0.31 ppm, with three additional peaks detected at 3.23 ppm, 1.44 ppm, and −1.70 ppm following further incubation. Chemical shift changes and line broadening, are consistent with non-coordinate interactions with HSA, likely with the hydrophobic binding domains of the protein. The protein-bound species are expected to have longer correlation times due to their association with HSA, and consequently a shorter transverse relaxation time (T_2) and corresponding larger linewidths.[54] These observations are in accord with previous reports of line broadening and chemical shift changes in the ^{19}F NMR of molecules with CF_3 groups interacting with HSA.[55] Furthermore, hydrophobic interactions with HSA have been identified for KP1019, NKP-1339, and other Keppler-type complexes.[3b, 5b, 8d, 10d] Comparison of these data with ^{19}F NMR from **1b** in PBS shows increased persistence of the first species and the absence of polynuclear species, demonstrating the impact the protein interactions have on the speciation of the complex.

Incubation of **1b** with HSA, also generated a sharp signal at 10.68 ppm, corresponding to free CF_3-Py ligand, as determined by comparison with the ^{19}F NMR spectrum of the isolated ligand in PBS (δ = 10.60 ppm, **Figure S15a**). The intensity of this signal increased with incubation, and after 24 hours showed two distinct components, the sharp peak assigned to free ligand in solution, and a broad feature shifted slightly down field. Incubation of the CF_3-Py ligand with HSA, produced a similar signal (δ = 10.76 ppm, **Figure S15a**), indicating a population of the ligand that is interacting with the protein. This provides additional evidence for non-coordinate interactions with HSA, likely promoted by the lipophilic CF_3 modified ligand.

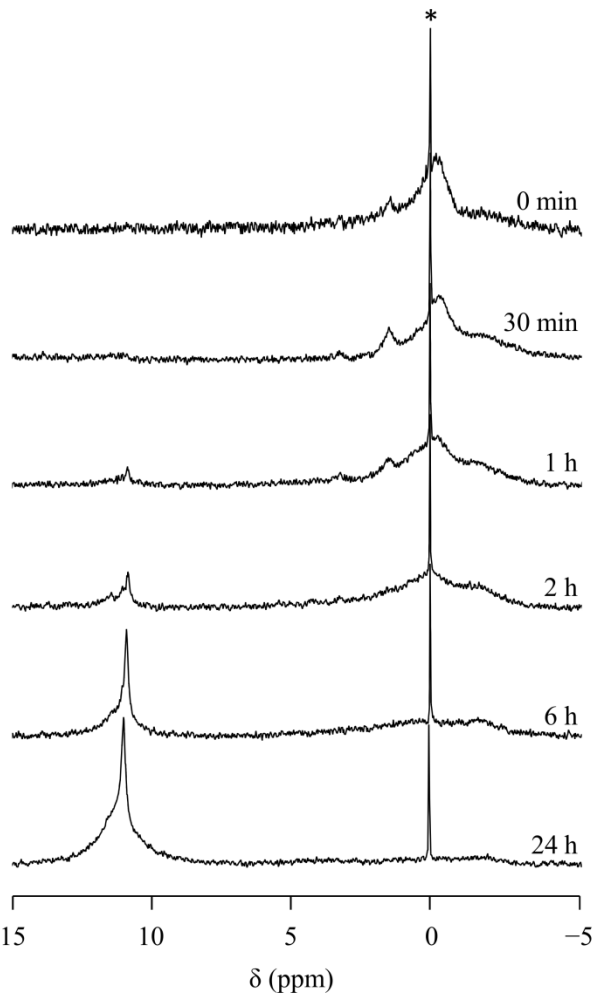

Figure 7. ^{19}F NMR spectra of **1b** (10 mM) incubated with HSA (2 mM) in PBS at 37 °C for 24 hours. The 0 min spectrum (2 min scans) has been adjusted to match the signal intensity of the subsequent time points (4 min scans) using an external trifluoroacetic acid signal. Chemical shifts were also calibrated using this signal, indicated by "*".

Interactions with HSA affect the ^{19}F NMR spectra of **2b** (**Figure S14a**) similarly to **1b**. As compared to the measurements in PBS, the signal from **2b** is broadened and shifted downfield. This is consistent with the complex forming non-coordinate interactions with the protein. Loss of this signal with incubation is accompanied by the increase in intensity of a sharp signal at δ = 13.84 ppm, and a broad peak at δ = 15.94 ppm, corresponding to free and protein-bound ligand populations. The loss of CF_3-Him from the Ru(III) complex is consistent with a previous study of the bis-imidazole complex KP418, which demonstrates that the complex can release imidazole ligands in the presence of biological nucleophiles.[39]

The solubility of **3b** in PBS is substantially improved in the presence of HSA, enabling NMR measurements. Similar enhancement of solubility has been reported for KP1019, and was associated with rapid formation of non-coordinate interactions with the hydrophobic binding domains of the protein.[10d] Initially, a very broad ^{19}F peak is observed at around 14 ppm, consistent with a mono-nuclear Ru(III) species bound non-coordinatively to HSA (**Figure S14b**). Further incubation gives signals from free CF_3-Hin (δ = 15.27 ppm) and another broad signal, likely from protein bound ligand.

Signals assignable to protein coordinated complexes, as detected by EPR (see below), were not observed in the ^{19}F NMR spectra of the complexes with HSA. These species likely have even longer correlation times than the non-coordinated protein-bound species, and may thus have very large line widths that make their signals unobservable.

Collectively, the ^{19}F NMR data demonstrate that these complexes readily form non-coordinate interactions with HSA, in accord with the EPR and UV-Vis studies discussed below. Furthermore, these data also show that the CF_3 modified ligands are readily lost in the presence of the HSA. Because of differences in sensitivity between the ^{19}F NMR measurements of the paramagnetic complexes and diamagnetic ligands, it is hard to assess the relative concentrations of these species. Nonetheless, these observations, and the absence of aggregated species in the presence of the protein, show that HSA can influence the speciation of these types of compounds, potentially influencing the active species that would be found in vivo.

EPR. Measurements of EPR spectra were performed on **1b**, **2b**, and **3b** following incubation with HSA in PBS for up to 24 hours at 37 °C (**Figures 8**, **S8**). Protein-bound fractions were isolated using centrifugal ultrafiltration so that EPR spectra were from HSA-associated Ru(III) species exclusively. At the earliest time point (0 min), the spectra of **1b** and **2b** were similar to those of the complexes in PBS and were simulated using the same parameters. Although EPR measurements of **3b** could not be made in PBS, greater solubility in the presence of HSA enabled spectra from protein-bound species to be detected with good signal-to-noise (**Figure S8c**). Signals at early incubation time points from **3b** were similar to those reported for the bis-indazole complex KP1019 in buffer.[10d] The observation of protein bound species, with the same ligand environments as solution species, indicates non-coordinate protein interactions, consistent with the NMR described above.

The overall EPR signal intensity from **1b** decreased considerably during incubation at 37 °C, indicating that protein bound species are not highly persistent (**Figure S8a**). However, spectral simulation identified four new signals that were not previously observed in PBS were still readily observed during the incubation period (**Figure S9**). The first two species detected with g = [2.45, 2.34, 1.32] (1b-HSA1), and g = [2.29, 2.24, 2.10] (1b-HSA2) were apparent as early as 30 minutes of incubation. After six hours of incubation, 1b-HSA1 was replaced by two more protein associated species, 1b-HSA3 with g = [2.53, 2.37, 1.32], and 1b-HSA4 with g = [2.35, 2.20, 1.83]. The formation of two HSA-coordinated species was also reported from EPR studies of $Na[RuCl_4Py_2]$ with HSA.[8d] Observation of two additional species at the longer incubation times used here is consistent with the subsequent loss of a CF_3-Py ligand following protein coordination, as indicated by ^{19}F NMR measurement of **1b** (see above).

The EPR spectra of complex **2b** with HSA are dominated by a single strong signal with g = [2.53, 2.34, 1.71] after 1 h of incubation. As shown in **Figure 8**, comparison of the EPR spectra of **2b** after 6 hours of incubation in PBS, and in the presence of HSA,

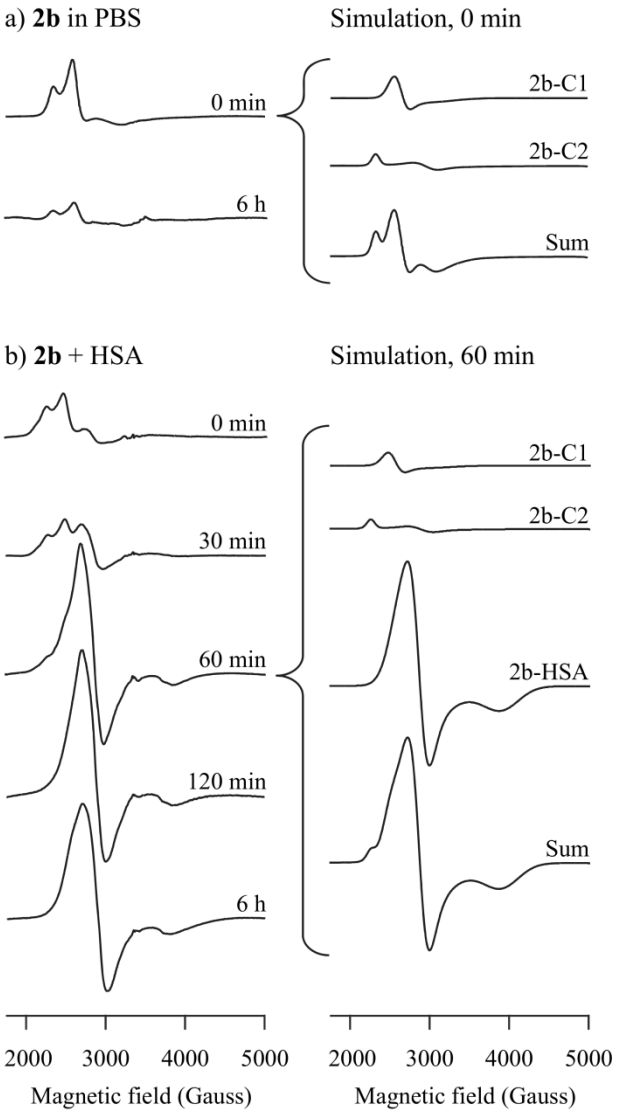

Figure 8. EPR spectra of **2b** incubated at 37 °C for 6 hours a) in PBS, and b) with HSA, and spectral simulations.

shows the unmistakable contribution of this Ru(III) species. This signal correlates with EPR spectra from the HSA-coordinated species of other Keppler-type complexes,[10d] demonstrating that **2b** also readily coordinates to the protein. A similar species is also observed for **3b**, 3b-HSA1 with g = [2.44, 2.26, 1.78] (**Figure S11**). These types of signals have been assigned to histidine coordinated complexes for KP1019 and KP418, with similar g values and characteristic large linewidths,[10d] indicating the same coordination mode for the CF_3 modified analogues of these compounds. In the case of **3b**, three additional minority species with narrow line widths are also observed: 3b-HSA2, $g_\perp$ = 2.29, $g_\parallel$ = 1.79; 3b-HSA3, g = [2.38, 2.29, 1.83]; and 3b-HSA4, g = [2.35, 2.24, 1.77], which indicate small contributions from other binding modes, possibly to different amino acid side chains.[10d]

Generally speaking, the EPR data indicate that the behavior of **1b**, **2b**, and **3b** are typical of Keppler-type complexes, with the rapid formation of non-coordinated species in the presence of HSA, followed by coordination to the protein at longer incubation times. However, comparison of the relative stability of their non-coordinated species shows a distinct trend. Spectral analysis by simulation demonstrates that non-coordinated species are ob-

served for **1b**, **2b**, and **3b** for up to 2 h, 1 h and 6 h respectively (**Figure 8, S9-S11**). This shows that the stability of non-coordinate interactions increases according to **2b** < **1b** < **3b**, which correlates with their hydrophobicity as determined by their log$D_{7.4}$ values. A previous study of pyridine-based NKP-1339 analogues demonstrated that stabilization of non-coordinate interactions with HSA can lead to increased cytotoxic activity,[8d] suggesting that addition of CF_3 groups could be beneficial to in vivo activation.

UV-Vis. The behavior of the complexes in the presence of HSA was evaluated using UV-Vis measurements in PBS at 37 °C over 2 hours (**Figures 9, S22-S27**). Complexes **2a**,**b** and **3a**,**b** displayed better solubility in the presence of HSA, as compared to PBS alone, with no evidence of baseline changes due to aggregation. The spectra of **1a**,**b** at early incubation time points are similar to those in PBS, indicating little change to the coordination environments of the complexes initially. These observations are consistent with the rapid formation of non-coordinate protein interactions, as detected by ^{19}F NMR and EPR (see above). At longer incubation times, the spectra of **1a**,**b** show a smaller contribution from the LMCT band at higher energy observed with ligand exchange in PBS. This is consistent with the ^{19}F NMR measurements of **1b** with HSA, which also suggest changes in the ligand-exchange processes of non-coordinatively bound complexes (see above). The UV-Vis data, combined with the ^{19}F NMR and EPR results, demonstrate that the presence of HSA not only improves solubility but can also modify the ligand-exchange behavior of these complexes.

Electrochemical measurements: The cyclic voltammograms of the sodium-compensated complexes **1b**, **2b**, **3b**, Na[RuCl$_4$Py$_2$], Na[RuCl$_4$Him$_2$], and NKP-1339 were measured in PBS (**Figures S34-S40**). Because of lower solubility, **3b** was initially dissolved in DMSO before addition to PBS, to give a 10% DMSO solution. To determine the solvent correction for this solution, NKP-1339 was also measured in the same solvent mixture, resulting in a 37 mV lowering of its formal reduction potential, $E^{\circ\prime}$, as compared to pure PBS. This correction was used to calculate the value of $E^{\circ\prime}$ for **3b** in PBS. Each complex showed a one-electron Ru(III) → Ru(II) redox couple with the different ligands having distinct effects on the values of $E^{\circ\prime}$ (**Table 1**).

Reduction potentials have been reported for NKP-1339 ($E^{\circ\prime}$ = 30 mV vs NHE) and KP418 ($E^{\circ\prime}$ = −160 mV vs NHE) in 0.2 M phosphate buffer, pH 7.[56] These values are similar to our results in PBS for NKP-1339 ($E^{\circ\prime}$ = 17 mV vs NHE) and Na[RuCl$_4$Him$_2$] ($E^{\circ\prime}$ = −188 mV). The reduction potential of each of the complexes can be estimated by Lever's empirical parameterization approach using additive contributions from the ligands.[57] As shown in Equation 3, the prediction of $E^{\circ\prime}$ uses an electrochemical ligand parameter, E_L, which correlates with the electron accepting characters of the ligands of redox-active metal complexes. The parameters S_M and I_M were determined by fitting ΣE_L and $E^{\circ\prime}$ values from various complexes for particular M^n/M^{n-1} redox couples.[57]

$$E^{\circ\prime} = S_M \cdot \sum E_L + I_M \qquad (3)$$

Parameters for Ru(III)(−1) → Ru(II)(−2) in aqueous phosphate buffer solutions have been reported by Reisner et al. with S_M = 0.88 and I_M = 0.46.[56] Using ligand parameters of $E_L(Cl^-)$ = −0.24,[57] E_L(indazole) = 0.26,[56] E_L(pyridine) = 0.25,[57] and E_L(imidazole) = 0.09,[58] we can thus calculate $E^{\circ\prime}$ for NKP-1339 (20 mV), Na[RuCl$_4$Py$_2$] (60 mV), and Na[RuCl$_4$Him$_2$] (−230 mV). These are all in reasonable agreement with the experimental values, particularly when solvent differences in our experimental conditions (PBS, pH 7.4) and the conditions used in establishing the Lever parameters (phosphate buffer, pH 7) are taken into account. For the complexes with CF_3 modified ligands, the values of E_L can be estimated using Equation 3 and $E_L(Cl^-)$. Using this approach, we calculate $E_L(CF_3\text{-Hin})$ = 0.34, $E_L(CF_3\text{-Py})$ = 0.35, and $E_L(CF_3\text{-Him})$ = 0.11. The value of $E_L(CF_3\text{-Py})$ is in agreement with a literature report of E_L = 0.32,[57] indicating the values calculated by this method are reliable. The electron-withdrawing CF_3 groups increase the overall electron-accepting properties of the ligands. This is reflected in higher values of E_L, corresponding to the higher reduction potentials of their respective Ru-complexes.

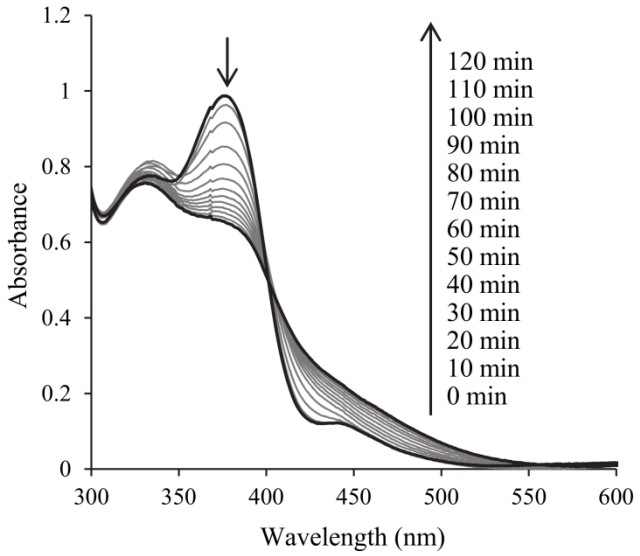

Figure 9. UV-Vis spectra of complex **1b** (200 μM) with HSA (100 μM) in PBS at 37 °C with incubation up to 24 hours.

The reduction potentials of Keppler-type complexes have been linked with their activities. The so-called "activation by reduction hypothesis suggests that generation of Ru(II) species in vivo may promote anticancer activity by increasing reactivity towards biomolecules.[1a, 59] This may be related to increased lability due to decreased affinity for π donor ligands and increased overall negative charge on the anionic ruthenium species.[1a, 60] Consequently, the loss of Cl^- ligands from these types of complexes is accelerated, which promotes potential interactions with proteins, DNA, and other biological targets. [47, 58] Evidence for this includes the greater affinity of KP1019 towards the DNA-modelling nucleotide, guanine monophosphate (GMP), in the presence of two equivalents of the reducing agent glutathione.[61] Similarly, studies of indazole Ru(III) complexes of the type $[Ru(III)Cl_{(6-n)}(Hind)n]^{(3-n)-}$ (n = 0-4), show that their cytotoxic activity against the SW480 colon carcinoma cell line correlates with their reduction potentials.[47] The redox activity of these types of complexes may also contribute to activation pathways related to oxidative stress. [3b] This concept has drawn particular attention because it suggests that targeted activation may be possible by selective reduction of Ru(III) complexes in hypoxic tumour environments.[59]

The compounds studied here with the highest reduction potentials, **1b**, **3b**, and NKP-1339, also exhibit cytotoxic activity while the other complexes are inactive (see below and **Table 1**). However, given that **1b** has a reduction potential 215 mV more positive than NKP-1339, and yet shows lower activity, we conclude that the reduction potential is not the main discriminator for the reactivity of these complexes. Furthermore, the reduction potentials of all of the complexes are within the potential range of physiological reduc-

ing agents such as glutathione ($E°'$ = −250 mV), indicating that their Ru(III) centers could be reduced in vivo. Aqueous ligand exchange of Cl^- will make reduction even more favorable, since Equation 3 parameterized for Ru(III)(0) → Ru(II)(−1) (S_M = 0.97, I_M = 0.04) [57] with $E_L(H_2O)$ = 0.04[57 57] predicts a significant increase in reduction potential. Thus, it seems likely that Ru(II) species play an important role in the activity all of the compounds studied in this report.

Biological testing: The sodium-compensated complexes **1b**, **2b**, and **3b**, as well as Na[$RuCl_4Py_2$], Na[$RuCl_4Him_2$], and NKP-1339 were tested for cytotoxicity against the chemosensitive human colon carcinoma HT-29 and the more chemoresistant non-small cell lung carcinoma A549 cell lines.[62] After the complexes were incubated with each of the cell lines for 72 hours, cell viability was assessed using a fluorescent cell-permeable nuclear marker (Hoescht 33342 nucleic acid stain) to determine total cell counts, and a cell-impermeable nuclear marker (ethidium homodimer I) was used to quantify dead cells. This enabled the "fraction affected" to be determined as the ratio of dead to live cells. Plots of fraction affected versus concentration (**Figure 10**, and **Figures S41, S42**) were then analyzed to determine IC_{50} values (**Table 1**) by fitting to a sigmoidal curve (**Figures S43-S49**).

Using this approach, IC_{50} values for NKP-1339 of 10 ± 1 μM against HT-29 cells and 50 ± 23 μM against A549 cells were determined. These results confirm the cytotoxic activity of this compound, as described in previous literature reports with IC_{50} values of 24.76[3a] and 156 μM[63] against these respective cell lines. This compares well with cisplatin against the HT-29 cell line which showed an IC_{50} of 9 ± 4 μM in our experiments (literature values of 20.36-25.4 μM[64]). Cisplatin was found to be more active against A549 cells with IC_{50} = 5 ± 1 μM (literature values of 2.36-5.95 μM[65]). The CF_3 functionalized analogue of NKP-1339, **3b**, also shows good activity against HT-29 cells with IC_{50} = 24 ± 4 μM. Interestingly, **3b** shows greater activity against the more chemoresistant cell line A549 than NKP-1339. An even greater effect from addition of CF_3 groups was observed for the pyridine complexes. While Na[$RuCl_4Py_2$] shows no activity against either cell line, its CF_3-Py analogue (**1b**) shows good activity against HT-29 cells with IC_{50} = 21 ± 3 μM. Neither of the imidazole complexes show measurable activity, which is consistent with previous reports that KP418 showed no cytotoxic activity against HT-29 cells.[3a]

Significantly, the three active compounds, **3b**, **1b**, and NKP-1339, also have the highest lipophilicity as shown by their values of log$D_{7.4}$ (**Table 1**). Whereas, the more hydrophilic compounds **2b**, Na[$RuCl_4Py_2$], and Na[$RuCl_4Him_2$] show no activity against either of the cell lines tested. This is particularly notable in the case of the pyridine complexes, where addition of the CF_3 group appears to raise log$D_{7.4}$ sufficiently to generate activity. This suggests that lipophilicity could be the major determinant of the cytotoxicity of Keppler type complexes. This is consistent with promotion of intercellular transport via passive diffusion, as indicated in previous studies of KP1019,[21] with the more lipophilic compounds having enhanced penetration of cell membranes.

Conclusion

Addition of CF_3 groups to the ligands of Keppler-type Ru(III) complexes has been studied as a means to modify their pharmacological behavior, and to install a spectroscopic handle for ^{19}F NMR studies. The ligands of the parent compounds, pyridine, imidazole, and indazole, and these ligands functionalized with CF_3 groups, provided a series of complexes (**Figure 1**) with a range of lipophilicities. From measurement of the distribution coefficient

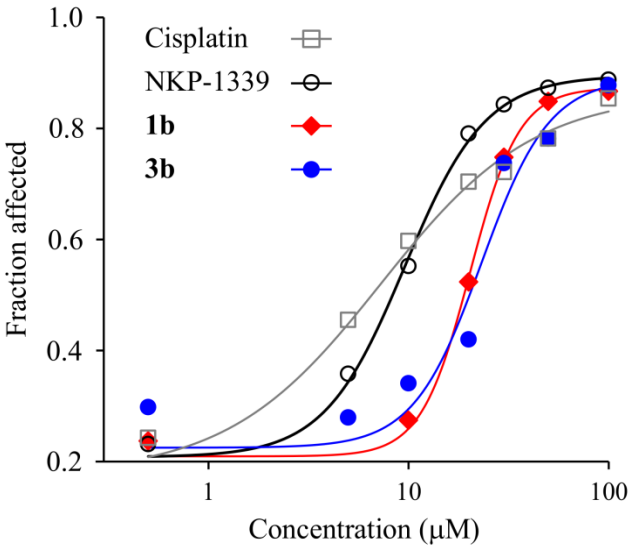

Figure 10: Cytotoxicity testing results of complexes **1b** (◆), **3b** (●), NKP-1339 (○), and cisplatin (□) against the HT-29 cell line, and sigmoidal fitting.

(log$D_{7.4}$) it was determined that the lipophilicity of the complexes varied as **3b** (bis-CF_3-Hin) > **1b** (bis-CF_3-Py) > NKP-1339 (bis-Hin) > **2b** (bis-CF_3-Him) > Na[$RuCl_4Py_2$] > Na[$RuCl_4Him_2$] (**Table 1**).

Studies of the ligand exchange behavior of the CF_3 modified complexes using ^{19}F NMR, EPR, and UV-Vis show distinct behavior in PBS. While **1b** shows step-wise aquation, followed by the formation of oligomeric species, **2b** is comparatively stable towards ligand exchange, and **3b** precipitates rapidly. Combined with previous studies of the aqueous solution behavior of the unsubstituted parent compounds,[8d, 10b-d] this demonstrates the important role that the axial heterocyclic ligands play in the aqueous solution behavior of these types of complexes. This is important since successful Keppler-type drug candidates are likely to be delivered by intravenous infusion, as in the case of the clinically tested compounds KP1019 and NKP-1339,[5c 3b] and so their behavior in aqueous solution prior to administration determines the actual species presented by the treatment.

Following infusion, interactions with serum proteins are prevalent for Keppler-type complexes.[3b, 10d, 66] Previous studies suggest that HSA is the primary target for these and other Ru(III) anticancer candidates in vivo,[67] with transferrin also possibly playing a role in delivering the complexes to tumors.[3b] Interactions with the main hydrophobic binding domains of HSA have been identified, suggesting that non-coordinate interactions with the protein are important in vivo.[10d, 25] Using fluorescence competition experiments we have shown here that the affinity of the CF_3-modified complexes and their unsubstituted parent compounds for hydrophobic binding site II of HSA correlates well with the lipophilicity of the compounds (**Table 1**). Furthermore, EPR, ^{19}F NMR and UV-Vis measurements confirm that these interactions occur readily in the presence of the protein. Thus, these observations confirm that Keppler-type complexes interact with the hydrophobic binding domains of HSA via non-coordinate interactions that are modulated by the lipophilicity of their axial ligands.

While non-coordinate interactions of Ru(III) complexes such as NKP-1339 and KP1019 are predominant after initial exposure to HSA, as time progresses coordinated species typically become more prevalent, eventually becoming predominant.[8d, 10d] As we

show here by EPR studies of the CF_3 functionalized compounds with HSA, the rate of transformation of non-coordinate to coordinate interactions increases as **2b** > **1b** > **3b**. This is inversely correlated with the lipophilicity of these compounds, indicating that increased stabilization of non-coordinate interactions at hydrophobic sites of HSA can inhibit formation of coordinated species. A previous study of KP1019 and NKP-1339 analogs suggests that stabilization of non-coordinate interactions may favor activity in vivo by maintaining greater bioavailability.[8d]

Studies of the cytotoxicity of the both the CF_3 functionalized complexes and their unmodified parent compounds towards the HT-29 and A549 cell lines also demonstrated the importance of lipophilicity. As we have shown here (**Table 1**), the three complexes with the highest distribution coefficients, **3b**, **1b**, and NKP-1339, show promising activity, while the other more hydrophilic compounds are relatively inactive. The most compelling result is the activity of the CF_3-Py complex, **1b**, which shows good activity (IC_{50} = 21 μM) against the HT-29 cell line. Whereas, the parent compound $Na[RuCl_4Py_2]$ is inactive against this cell line. We suggest that greater lipophilicity may enhance passive diffusion of the complexes through cell membranes, leading to greater intracellular ruthenium concentrations and enhanced activity.

Previous studies of Ru(III) complexes have implicated reduction potentials as a factor affecting activity. This is predicated on the premise that generation of Ru(II) species may be an important part of their mechanism of activation.[1a, 56, 59-60] Measurement of $E^{\circ\prime}$ for both the parent compounds and the CF_3 modified complexes (**Table 1**) do show that the active compounds have higher reduction potentials. Furthermore, addition of CF_3 groups increases the reduction potentials of the complexes due to the more electron accepting nature of the ligands. However, the reduction potentials of all the complexes are within the physiological window, suggesting they could all be found in the Ru(II) state in the in vitro studies, and there is no obvious trend with regards to reduction potential and the IC_{50} values of the active compounds. Nonetheless, we cannot exclude this as having some contribution to the observed activities.

As a whole, this work demonstrates that trifluoromethylation could be a useful general approach for influencing the pharmacological behavior of Ru(III) anticancer compounds both through enhancing transport by HSA and also by improving cytotoxic activity. Furthermore, addition of CF_3 groups enables ^{19}F NMR studies of ligand exchange processes and protein interactions.

ASSOCIATED CONTENT

Supporting Information. CCDC-1453157 (**1a**), CCDC-1453158 (**2c**), and CCDC-1453159 (**3c**) contain the supplementary crystallographic data for this paper. These data can be obtained free of charge from The Cambridge Crystallographic Data Centre via www.ccdc.cam.ac.uk/data_request/cif.

Crystal data, details of data collection and refinement, and Ru-ligand bond lengths. Fluorescence emission spectra. UV-Vis spectra for determination of log$D_{7.4}$. EPR spectra and simulation parameters for complexes in PBS and with HSA. ^{19}F NMR spectra of incubation in PBS as well as fluorinated ligands in PBS and with HSA. UV-Vis spectra of complexes in PBS and with HSA. Cyclic voltammograms. Dose response data and fitting for the HT-29 and A549 cell lines. This material is available free of charge via the Internet at http://pubs.acs.org.

AUTHOR INFORMATION

Corresponding Author

*E-mail: cwalsby@sfu.ca

Notes

The authors declare no competing financial interest.

ACKNOWLEDGMENTS

Financial support for this work was provided by The Natural Sciences and Engineering Research Council of Canada and Simon Fraser University. K.E.P. acknowledges support from a Vanier Canada Graduate Scholarship.

ABBREVIATIONS

5-FU	5-fluorouracil
CF_3	Trifluoromethyl
Cisplatin	*cis*-diamminedichloridoplatinum(II)
D	Distribution coefficient
DG	Dansylglycine
EPR	Electron paramagnetic resonance
HSA	Human serum albumin
IC_{50}	Half maximal inhibitory concentration
Him	Imidazole
Hin	Indazole
K′	Conditional binding constant at site II
KP1019	Indazolium [*trans*-$RuCl_4$(1*H*-indazole)$_2$]
KP418	Imidazolium [*trans*-$RuCl_4$(1*H*-imidazole)$_2$]
NHE	Normal hydrogen electrode
NKP-1339	Sodium [*trans*-$RuCl_4$(1*H*-indazole)$_2$]
PBS	Phosphate buffered saline
PNP	Bis(triphenylphosphine)iminium ion
Py	Pyridine
TFA	Trifluoroacetic acid

REFERENCES

(1) a) Clarke, M. J., *Coord. Chem. Rev.* **2003**, *236*, 209-233; b) Alessio, E.; Mestroni, G.; Bergamo, A.; Sava, G., *Curr. Top. Med. Chem.* **2004**, *4*, 1525-1535; c) Yan, Y. K.; Melchart, M.; Habtemariam, A.; Sadler, P. J., *Chem. Commun.* **2005**, 4764-4776; d) Ang, W. H.; Dyson, P. J., *Eur. J. Inorg. Chem.* **2006**, 4003-4018; e) Jakupec, M. A.; Galanski, M.; Arion, V. B.; Hartinger, C. G.; Keppler, B. K., *Dalton Trans.* **2008**, 183-194; f) Levina, A.; Mitra, A.; Lay, P. A., *Metallomics* **2009**, *1*, 458-470; g) Antonarakis, E. S.; Emadi, A., *Cancer Chemother. Pharmacol.* **2010**, *66*, 1-9; h) Bergamo, A.; Sava, G., *Dalton Trans.* **2011**, *40*, 7817-7823; i) Bratsos, I.; Gianferrara, T.; Alessio, E.; Hartinger, C. G.; Jakupec, M. A.; Keppler, B. K. *Ruthenium and other non-platinum anticancer compounds*, Wiley-VCH Verlag GmbH & Co. KGaA: 2011; pp 151-174.
(2) a) Keppler, B. K.; Henn, M.; Juhl, U. M.; Berger, M. R.; Niebl, R.; Wagner, F. E., *Prog. Clin. Biochem. Med.* **1989**, *10*, 41-69; b) Hartinger, C. G.; Zorbas-Seifried, S.; Jakupec, M. A.; Kynast, B.; Zorbas, H.; Keppler, B. K., *J. Inorg. Biochem.* **2006**, *100*, 891-904.
(3) a) Kapitza, S.; Pongratz, M.; Jakupec, M. A.; Heffeter, P.; Berger, W.; Lackinger, L.; Keppler, B. K.; Marian, B., *J. Cancer. Res. Clin. Oncol.* **2005**, *131*, 101-110; b) Trondl, R.; Heffeter, P.; Kowol, C. R.; Jakupec, M. A.; Berger, W.; Keppler, B. K., *Chem. Sci.* **2014**, *5*, 2925-2932.
(4) Sava, G.; Alessio, E.; Bergamo, A.; Mestroni, G., *Top. Biol. Inorg. Chem.* **1999**, *1*, 143-169.
(5) a) Rademaker-Lakhai, J. M.; Van Den Bongard, D.; Pluim, D.; Beijnen, J. H.; Schellens, J. H. M., *Clin. Cancer Res.* **2004**, *10*, 3717-3727; b) Hartinger, C. G.; Jakupec, M. A.; Zorbas-Seifried, S.; Groessl, M.; Egger, A.; Berger, W.; Zorbas, H.; Dyson, P. J.; Keppler, B. K., *Chem. Biodiversity* **2008**, *5*, 2140-2155; c) Lentz, F.; Drescher, A.; Lindauer, A.; Henke, M.; Hilger, R. A.; Hartinger, C. G.; Scheulen, M. E.; Dittrich, C.; Keppler, B. K.; Jaehde, U., *Anti-Cancer Drugs* **2009**, *20*, 97-103; d) Leijen, S.; Burgers, S. A.; Baas, P.; Pluim, D.; Tibben, M.; van Werkhoven, E.; Alessio, E.; Sava, G.; Beijnen, J. H.; Schellens, J. H. M., *Invest. New Drugs* **2015**, *33*, 201-214.
(6) Keppler, B. K.; Rupp, W., *J. Cancer Res. Clin. Oncol.* **1986**, *111*, 166-168.

(7) Garzon, F. T.; Berger, M. R.; Keppler, B. K.; Schmaehl, D., *Cancer Chemother. Pharmacol.* **1987**, *19*, 347-349.
(8) a) Keppler, B. K.; Balzer, W.; Seifried, V., *Arzneim.-Forsch.* **1987**, *37*, 770-771; b) Arion, V. B.; Reisner, E.; Fremuth, M.; Jakupec, M. A.; Keppler, B. K.; Kukushkin, V. Y.; Pombeiro, A. J. L., *Inorg. Chem.* **2003**, *42*, 6024-6031; c) Mura, P.; Piccioli, F.; Gabbiani, C.; Camalli, M.; Messori, L., *Inorg. Chem.* **2005**, *44*, 4897-4899; d) Webb, M. I.; Wu, B.; Jang, T.; Chard, R. A.; Wong, E. W. Y.; Wong, M. Q.; Yapp, D. T. T.; Walsby, C. J., *Chem. Eur. J.* **2013**, *19*, 17031-17042.
(9) a) Anderson, C.; Beauchamp, A. L., *Can. J. Chem.* **1995**, *73*, 471-482; b) Keppler, B. K.; Pieper, T. *Studies into the mode of action of trans-HInd[RuCl$_4$(ind)$_2$] and trans-HIm[RuCl$_4$(im)$_2$]*, Bioinorganic Chemistry, Trautwein, A. X., Ed. Wiley-VCH Verlag GmbH: 1997; pp 123-128; c) Reedijk, J., *Platinum Met. Rev.* **2008**, *52*, 2-11.
(10) a) Smith, C. A.; Sutherland-Smith, A. J.; Keppler, B. K.; Kratz, F.; Baker, E. N., *J. Biol. Inorg. Chem.* **1996**, *1*, 424-431; b) Groessl, M.; Hartinger, C. G.; Dyson, P. J.; Keppler, B. K., *J. Inorg. Biochem.* **2008**, *102*, 1060-1065; c) Cebrian-Losantos, B.; Reisner, E.; Kowol, C. R.; Roller, A.; Shova, S.; Arion, V. B.; Keppler, B. K., *Inorg. Chem.* **2008**, *47*, 6513-6523; d) Cetinbas, N.; Webb, M. I.; Dubland, J. A.; Walsby, C. J., *J. Biol. Inorg. Chem.* **2010**, *15*, 131-145; e) Antony, S.; Aitken, J.; Vogt, S.; Lai, B.; Brown, T.; Spiccia, L.; Harris, H., *J. Biol. Inorg. Chem.* **2013**, *18*, 845-853.
(11) a) Bergamo, A.; Masi, A.; Jakupec, M. A.; Keppler, B. K.; Sava, G., *Met. Based Drugs* **2009**, *2009*, 681270; b) Kersten, L.; Braunlich, H.; Keppler, B. K.; Gliesing, C.; Wendelin, M.; Westphal, J., *J. Appl. Toxicol.* **1998**, *18*, 93-101; c) Keppler, B. K.; Pieper, T., Studies into the mode of action of *trans*-HInd[RuCl$_4$(ind)$_2$] and *trans*-HIm[RuCl$_4$(im)$_2$], In *Bioinorganic Chemistry: Transition Metals in Biology and Their Coordination Chemistry*, Trautwein, A. X., Ed. Wiley-VCH: Weinheim, Germany, 1997.
(12) a) Park, B. K.; Kitteringham, N. R.; O'Neill, P. M., *Annu. Rev. Pharmacol. Toxicol.* **2001**, *41*, 443-470; b) Purser, S.; Moore, P. R.; Swallow, S.; Gouverneur, V., *Chem. Soc. Rev.* **2008**, *37*, 320-330; c) Ojima, I., *J. Org. Chem.* **2013**, *78*, 6358-6383.
(13) a) Isanbor, C.; O'Hagan, D., *J. Fluorine Chem.* **2006**, *127*, 303-319; b) Hagmann, W. K., *J. Med. Chem.* **2008**, *51*, 4359-4369; c) O'Hagan, D., *J. Fluorine Chem.* **2010**, *131*, 1071-1081; d) Wang, J.; Sanchez-Rosello, M.; Acena, J. L.; del Pozo, C.; Sorochinsky, A. E.; Fustero, S.; Soloshonok, V. A.; Liu, H., *Chem. Rev.* **2014**, *114*, 2432-2506.
(14) Longley, D. B.; Harkin, D. P.; Johnston, P. G., *Nat. Rev. Cancer* **2003**, *3*, 330-338.
(15) Muller, K.; Faeh, C.; Diederich, F., *Science* **2007**, *317*, 1881-1886.
(16) Ruiz-Cabello, J.; Barnett, B. P.; Bottomley, P. A.; Bulte, J. W. M., *NMR Biomed.* **2011**, *24*, 114-129.
(17) Ametamey, S. M.; Honer, M.; Schubiger, P. A., *Chem. Rev. (Washington, DC, U. S.)* **2008**, *108*, 1501-1516.
(18) Yu, J.-X.; Hallac, R. R.; Chiguru, S.; Mason, R. P., *Prog. Nucl. Magn. Reson. Spectrosc.* **2013**, *70*, 25-49.
(19) Chen, H.; Viel, S.; Ziarelli, F.; Peng, L., *Chem. Soc. Rev.* **2013**, *42*.
(20) a) Gerig, J. T., *Prog. Nucl. Magn. Reson. Spectrosc.* **1994**, *26*, 293-370; b) Yu, J.-x.; Kodibagkar, V. D.; Cui, W.; Mason, R. P., *Curr. Med. Chem.* **2005**, *12*, 819-848.
(21) a) Levina, A.; Aitken, J. B.; Gwee, Y. Y.; Lim, Z. J.; Liu, M.; Singharay, A. M.; Wong, P. F.; Lay, P. A., *Chem. Eur. J.* **2013**, *19*, 3609-3619; b) Webb, M. I.; Walsby, C. J., *Metallomics* **2013**, *5*, 1624-1633.
(22) Pongratz, M.; Schluga, P.; Jakupec, M. A.; Arion, V. B.; Hartinger, C. G.; Allmaier, G.; Keppler, B. K., *J. Anal. At. Spectrom.* **2004**, *19*, 46-51.
(23) Hudej, R.; Miklavcic, D.; Cemazar, M.; Todorovic, V.; Sersa, G.; Bergamo, A.; Sava, G.; Martincic, A.; Scancar, J.; Keppler, B. K.; Turel, I., *J. Membr. Biol.* **2014**, *247*, 1239-1251.
(24) Van de Waterbeemd, H.; Smith, D. A.; Jones, B. C., *J. Comput.-Aided Mol. Des.* **2001**, *15*, 273-286.
(25) Doemoetoer, O.; Hartinger, C. G.; Bytzek, A. K.; Kiss, T.; Keppler, B. K.; Enyedy, E. A., *J. Biol. Inorg. Chem.* **2013**, *18*, 9-17.
(26) Webb, M. I.; Chard, R. A.; Al-Jobory, Y. M.; Jones, M. R.; Wong, E. W. Y.; Walsby, C. J., *Inorg. Chem.* **2012**, *51*, 954-966.
(27) Keppler, B. K.; Rupp, W.; Juhl, U. M.; Endres, H.; Niebl, R.; Balzer, W., *Inorg. Chem.* **1987**, *26*, 4366-4370.
(28) Peti, W.; Pieper, T.; Sommer, M.; Keppler, B. K.; Giester, G., *Eur. J. Inorg. Chem.* **1999**, *1999*, 1551-1555.
(29) Sheldrick, G., *Acta Crystallogr. A* **2015**, *71*, 3-8.
(30) Sheldrick, G., *Acta Crystallogr. C* **2015**, *71*, 3-8.
(31) a) Hubschle, C. B.; Sheldrick, G. M.; Dittrich, B., *J. Appl. Crystallogr.* **2011**, *44*, 1281-1284; b) Due to systematic error, reflections (−1 9 2 and −10 −6 1) were omitted for complex **2c** and reflections (−1 0 2, 2 −1 1, 1 −1 2, −1 −1 3, −2 1 0, −1 1 2, and –2 0 2) were omitted for complex **3c**. .
(32) Farrugia, L., *J. Appl. Crystallogr.* **2012**, *45*, 849-854.
(33) Fenn, T. D.; Ringe, D.; Petsko, G. A., *J. Appl. Crystallogr.* **2003**, *36*, 944-947.
(34) Glasoe, P. K.; Long, F. A., *J. Phys. Chem.* **1960**, *64*, 188-190.
(35) Stoll, S.; Schweiger, A., *J. Magn. Reson.* **2006**, *178*, 42-55.
(36) Lakowicz, J. R., *Principles of Fluorescence Spectroscopy*. 3rd ed.; Springer: New York, 2006.
(37) a) OECD, *Test No. 107: Partition Coefficient (n-octanol/water): Shake Flask Method*. OECD Publishing: 1995; b) Rathgeb, A.; Böhm, A.; Novak, M. S.; Gavriluta, A.; Dömötör, O.; Tommasino, J. B.; Enyedy, É. A.; Shova, S.; Meier, S.; Jakupec, M. A.; Luneau, D.; Arion, V. B., *Inorg. Chem.* **2014**, *53*, 2718-2729.
(38) Blakemore, J. D.; Schley, N. D.; Balcells, D.; Hull, J. F.; Olack, G. W.; Incarvito, C. D.; Eisenstein, O.; Brudvig, G. W.; Crabtree, R. H., *J. Am. Chem. Soc.* **2010**, *132*, 16017-16029.
(39) Hartmann, M.; Lipponer, K.-G.; Keppler, B. K., *Inorg. Chim. Acta* **1998**, *267*, 137-141.
(40) Villarreal-Salinas, B. E.; Schlemper, E. O., *J. Cryst. Mol. Struct.* **1978**, *8*, 217-237.
(41) Testa, B.; Crivori, P.; Reist, M.; Carrupt, P.-A., *Perspect. Drug Discov.* **2000**, *19*, 179-211.
(42) Kah, M.; Brown, C. D., *Chemosphere* **2008**, *72*, 1401-1408.
(43) Bhal, S. K.; Kassam, K.; Peirson, I. G.; Pearl, G. M., *Mol. Pharm.* **2007**, *4*, 556-560.
(44) Lipinski, C. A.; Lombardo, F.; Dominy, B. W.; Feeney, P. J., *Adv. Drug Deliver. Rev.* **1997**, *23*, 3-25.
(45) Li, X.-C.; Liu, K.-G.; Qin, D.-A.; Cheng, C.-C.; Chen, B.-X.; Hu, M.-L., *J. Mol. Struct.* **2012**, *1027*, 104-110.
(46) Lipponer, K.-G.; Vogel, E.; Keppler, B. K., *Met.-Based Drugs* **1996**, *3*, 243-260.
(47) Jakupec, M. A.; Reisner, E.; Eichinger, A.; Pongratz, M.; Arion, V. B.; Galanski, M.; Hartinger, C. G.; Keppler, B. K., *J. Med. Chem.* **2005**, *48*, 2831-2837.
(48) Kratz, F.; Hartmann, M.; Keppler, B.; Messori, L., *J. Biol. Chem.* **1994**, *269*, 2581-2588.
(49) Ni Dhubhghaill, O. M.; Hagen, W. R.; Keppler, B. K.; Lipponer, K.-G.; Sadler, P. J., *J. Chem. Soc., Dalton Trans.* **1994**, 3305-10.
(50) a) Colmenarejo, G., *Med. Res. Rev.* **2003**, *23*, 275-301; b) Quinlan, G. J.; Martin, G. S.; Evans, T. W., *Hepatology* **2005**, *41*, 1211-1219.
(51) Sulyok, M.; Hann, S.; Hartinger, C. G.; Keppler, B. K.; Stingeder, G.; Koellensperger, G., *J. Anal. At. Spectrom.* **2005**, *20*, 856-863.
(52) Muller, N.; Lapicque, F.; Drelon, E.; Netter, P., *J. Pharm. Pharmacol.* **1994**, *46*, 300-304.
(53) Webb, M. I.; Walsby, C. J., *Dalton Trans.* **2015**, *44*, 17482-17493.
(54) Claridge, T. D. W., *High-resolution NMR techniques in organic chemistry*. Pergamon: Amsterdam; New York, 1999; Vol. 19.
(55) a) Kitamura, K.; Kume, M.; Yamamoto, M.; Takegami, S.; Kitade, T., *J. Pharmaceut. Biomed.* **2004**, *36*; b) Kitamura, K.; Omran, A.; Takegami, S.; Tanaka, R.; Kitade, T., *Anal Bioanal Chem* **2007**, *387*.
(56) Reisner, E.; Arion, V. B.; Guedes da Silva, M. F. C.; Lichtenecker, R.; Eichinger, A.; Keppler, B. K.; Kukushkin, V. Y.; Pombeiro, A. J. L., *Inorg. Chem.* **2004**, *43*, 7083-7093.
(57) Lever, A. B. P., *Inorg. Chem.* **1990**, *29*, 1271-1285.
(58) Clarke, M. J.; Bailey, V. M.; Doan, P. E.; Hiller, C. D.; LaChance-Galang, K. J.; Daghlian, H.; Mandal, S.; Bastos, C. M.; Lang, D., *Inorg. Chem.* **1996**, *35*, 4896-4903.
(59) Reisner, E.; Arion, V. B.; Keppler, B. K.; Pombeiro, A. J. L., *Inorg. Chim. Acta* **2008**, *361*, 1569-1583.
(60) Jungwirth, U.; Kowol, C. R.; Keppler, B. K.; Hartinger, C. G.; Berger, W.; Heffeter, P., *Antioxid. Redox Sign.* **2011**, *15*, 1085-1127.
(61) Schluga, P.; Hartinger, C. G.; Egger, A.; Reisner, E.; Galanski, M.; Jakupec, M. A.; Keppler, B. K., *Dalton Trans.* **2006**, 1796-1802.
(62) Cole, S. P. C., *Cancer Chemother. Pharmacol.* **1986**, *17*, 259-263.
(63) Kuhn, P. S.; Pichler, V.; Roller, A.; Hejl, M.; Jakupec, M. A.; Kandioller, W.; Keppler, B. K., *Dalton Trans.* **2015**, *44*, 659-668.
(64) a) Zirvi, K. A.; Hill, G. J., *J. Surg. Oncol.* **1988**, *38*, 88-93; b) Pendyala, L.; Creaven, P. J., *Cancer Res.* **1993**, *53*, 5970-5976; c) Tardito, S.; Isella, C.; Medico, E.; Marchiò, L.; Bevilacqua, E.; Hatzoglou, M.; Bussolati, O.; Franchi-Gazzola, R., *J. Biol. Chem.* **2009**, *284*, 24306-24319.
(65) a) Wu, J.; Hu, C.-p.; Gu, Q.-h.; Li, Y.-p.; Song, M., *Acta Pharmacol. Sin.* **2009**, *31*, 93-101; b) Barr, M. P.; Gray, S. G.; Hoffmann, A. C.; Hilger, R. A.; Thomale, J.; O'Flaherty, J. D.; Fennell, D. A.; Richard, D.; O'Leary, J. J.; O'Byrne, K. J., *PLoS ONE* **2013**, *8*, e54193; c) Lopez-Ayllon, B. D.; Moncho-Amor, V.; Abarrategi, A.; de Cáceres, I. I.; Castro-

Carpeño, J.; Belda-Iniesta, C.; Perona, R.; Sastre, L., *Cancer Med.* **2014**, *3*, 1099-1111.
(66) a) Piccioli, F.; Sabatini, S.; Messori, L.; Orioli, P.; Hartinger, C. G.; Keppler, B. K., *J. Inorg. Biochem.* **2004**, *98*, 1135-1142; b) Hartinger, C. G.; Hann, S.; Koellensperger, G.; Sulyok, M.; Groessl, M.; Timerbaev, A. R.; Rudnev, A. V.; Stingeder, G.; Keppler, B. K., *Int. J. Clin. Pharmacol. Ther.* **2005**, *43*, 583-585.
(67) Kratz, F.; Mulinacci, N.; Messori, L.; Bertini, I.; Keppler, B. K., Kinetic, spectroscopic and LPLC studies of the interactions of antitumor ruthenium(III) complexes with serum-proteins, In *Metal Ions in Biology and Medicine*, *Vol 2*, Anastassopoulou, J.; Collery, P.; Etienne, J. C.; Theophanides, T., Eds., John Libbey Eurotext Ltd: Montrouge, 1992; Vol. 2.

For Table of Contents Only

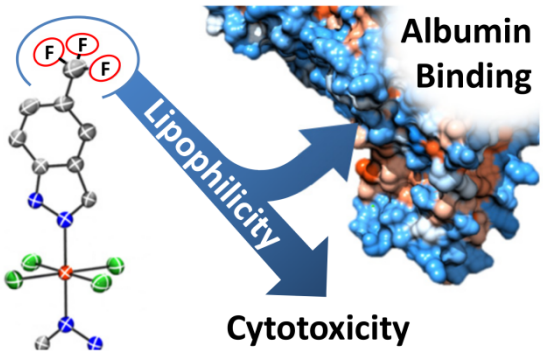

CF_3 derivatives of the anticancer Ru(III) complexes KP1019, NKP-1339, and their imidazole and pyridine analogues show enhanced lipophilicity, albumin interactions, and cytotoxicity

Stephanie. W. Chang,[†] Andrew R. Lewis,[†] Kathleen E. Prosser,[†] John R. Thompson,[†] Margarita Gladkikh,[†] Marcel B. Bally,[‡] Jeffrey J. Warren,[†] and Charles J. Walsby[†,*]

Trifluoromethyl analogues of "Keppler-type" Ru(III) complexes have been synthesized to probe the effect of lipophilicity on the pharmacological properties of these types of compounds. The inclusion of ^{19}F atoms also provides a spectroscopic handle for NMR studies. Increased complex lipophilicity promotes non-coordinate interactions with albumin, and coordination to the protein is also observed. The most lipophilic compounds exhibit the highest in vitro cytotoxicity, indicating that this is an important factor in the anticancer activity for complexes of this type.